*J. Fluid Mech.* (1999), *vol.* 378, *pp.* 233–267. Printed in the United Kingdom



# On the formation of Moore curvature singularities in vortex sheets

By STEPHEN J. COWLEY[1], GREG R. BAKER[2] AND SALEH TANVEER[2]

[1]Department of Applied Mathematics and Theoretical Physics, University of Cambridge, Silver Street, Cambridge CB3 9EW, UK

[2]Department of Mathematics, Ohio State University, Columbus, OH 43210-1174, USA

(Received 29 April 1997 and in revised form 25 August 1998)

Moore (1979) demonstrated that the cumulative influence of small nonlinear effects on the evolution of a slightly perturbed vortex sheet is such that a curvature singularity can develop at a large, but finite, time. By means of an analytical continuation of the problem into the complex spatial plane, we find a consistent asymptotic solution to the problem posed by Moore. Our solution includes the shape of the vortex sheet as the curvature singularity forms. Analytic results are confirmed by comparison with numerical solutions. Further, for a wide class of initial conditions (including perturbations of finite amplitude), we demonstrate that $\frac{3}{2}$-power singularities can spontaneously form at $t = 0+$ in the complex plane. We show that these singularities propagate around the complex plane. If two singularities collide on the real axis, then a point of infinite curvature develops on the vortex sheet. For such an occurrence we give an asymptotic description of the vortex-sheet shape at times close to singularity formation.

## 1. Introduction

This paper is concerned with the asymptotic description of inviscid fluid flows with vortex sheets. *Inter alia*, we present a consistent asymptotic solution for the formation of Moore curvature singularities. The methodology that we adopt has application to other ill-posed free-surface flows.

### 1.1. *Kelvin–Helmholtz instability*

One of the generic features of shear flows at high Reynolds numbers is Kelvin–Helmholtz (K–H) instability. Well known examples where K–H waves develop include (*a*) the instability of the mixing layer between two parallel streams of different speed, and (*b*) the instability of the vortex sheet centred on the dividing streamline of a separated flow. Further, it has been suggested that K–H instability plays a role in maintaining turbulent flow by causing the break-up of shear layers (e.g. Lundgren 1982).

A key feature of K–H instability on an infinitesimally thin vortex sheet is that linear, sinusoidal, disturbances with a wavenumber $k$, have a growth rate proportional to $k$. Hence, because there is no length scale in the problem, there is no fastest growing wave and the linear problem is ill-posed. The solution to a linearized problem for the shape of the vortex sheet can, therefore, develop a singularity within a finite time even if the initial data are analytic (Saffman & Baker 1979).

In order to determine whether such a finite-time singularity is an artifact of linearization, Moore (1979) studied the nonlinear evolution of a vortex sheet for a small initial disturbance that was sinusoidal. He found that the inclusion of nonlinear effects did not prevent the formation of a singularity after a finite time. In particular he predicted that close to the singularity, the curvature of the sheet was proportional to $|\Gamma - \Gamma_s|^{-1/2}$, where $\Gamma$ is the circulation in the sheet measured from a fixed reference particle and $\Gamma_s$ is the position of singularity. Although Moore's analysis involves an approximation, the result that the curvature of the vortex sheet develops a singularity after a finite time was supported by Meiron, Baker & Orszag (1982, henceforth referred to as MBO), who analysed a power series solution using series extension techniques. This result was confirmed by a direct numerical solution of the Birkhoff–Rott boundary integral equation which describes the motion of the sheet (Krasny 1986*a*); the growth of rounding error due to the linear ill-posedness of the problem was controlled by spectral filtering. Shelley (1992) refined and extended these calculations. For the most part he found the same type of singularity, but could not obtain precise agreement with certain details of Moore's (1979) analysis.

An improved understanding of the formation of the singularity is important because the K–H instability mechanism can lead to curvature singularities in problems that at first sight look as if they are unaffected by K–H instability. For instance, Pugh (1989) studied the rise of two-dimensional, inviscid bubbles under a Boussinesq approximation. For bubbles that start from rest, he showed numerically that after a finite time, a curvature singularity develops at the interface between the two fluids. The singularity arises because the vortex sheet that exists at the interface can support K–H instability (although it should be emphasized that there is no visual evidence of short-wavelength waves in the interface shape prior to the formation of the curvature singularity). Pugh (1989) has similarly demonstrated that a curvature singularity can form when a point-vortex pair approaches a stably stratified interface, while both he and Siegel (1990) have shown that a singularity can form in the Rayleigh–Taylor instability of an interface between two fluids of different, non-zero density. Indeed, Siegel (1990, private communication) has noted that singularities are almost certain to form in unsteady interfacial wave problems, the exception seems to be when the interface is between a vacuum and a fluid (see also Ebin 1987, 1988; Tanveer 1993). These conclusions are supported by Baker, Caflisch & Siegel (1993) who have performed numerical calculations for a wide range of Atwood numbers for the Rayleigh–Taylor instability problem. We also note that singularity formation is not restricted to two dimensions. For instance, Pugh (1989) has shown that a singularity forms on a rising, axisymmetric, Boussinesq bubble, while Nie & Baker (1998) and Nitsche (1998) have demonstrated singularity formation in other axisymmetric problems. There is also some evidence that singularities form on three-dimensional vortex sheets (Ishihara & Kaneda 1994, 1995).

The precise nature of the solution after singularity formation in any of these cases has yet to be elucidated in detail. However, it is known for single-signed vortex sheets both that a classical weak solution to the two-dimensional Euler equations exists for all time (Delort 1991; Majda 1993), and that solutions based on the vortex 'blob' method converge in the limit of zero blob size to classical weak solutions (Liu & Xin 1995). Further, numerical solutions of models invoking regularization agents such as finite-sheet thickness (e.g. Moore 1978; Baker & Shelley 1990), blobs (e.g. Krasny 1986*b*) or viscosity (e.g. Tryggvason, Dahm & Sbeih 1991), have been found to converge to the vortex-sheet solution at times before a singularity forms in the vortex-sheet model; while after that time, the regularized solutions develop spirals

that appear to be self-similar.† Our hope is that the following analysis, especially that in § 5, will be a contributory step in understanding, *inter alia*, the formation and evolution of these rolled-up spirals in the limit of vanishingly small sheet thickness, blob size or viscosity. Indeed, if the correct weak limit can be identified, then it may be possible to develop modified numerical methods for vortex-sheet motion that retain the vortex sheet as a useful approximation of high-Reynolds-number thin shear layers at times after singularity formation.

### 1.2. *Applicability of the vortex-sheet model*

Since the vortex-sheet model is mathematically ill-posed for general classes of initial conditions, a natural question to ask is under what circumstances does the vortex-sheet model provide useful approximations of physical behaviour? Certainly vortex-sheet solutions can only be asymptotic approximations if the dominant length scale of the flow is much larger than the thickness of the assumed underlying shear layer; we will assume that this condition is satisfied. We also know that the vortex-sheet problem is well-posed for a finite time if the initial data lie in a certain class of analytic functions (Sulem *et al.* 1981; Caflisch & Orellana 1986; Duchon & Robert 1988). We believe that our work is relevant to this class of analytic initial conditions, and moreover we note that this class of initial conditions includes 'noisy' initial conditions as long as the noise can be described by small, appropriate analytic perturbations. For a discussion of the latter point in the context of noise in numerical solutions see the work of Caflisch & Lowengrub (1989). However, when such analytic noise is present (even if of relatively small amplitude), it can play a key rôle in singularity formation if the strip of analyticity in the complex $\Gamma$-plane of the noise is thin.

Finally in our discussion of applicability, we note that if an initial condition is contaminated by noise that is non-analytic (e.g. the Fourier transform of the noise decays in wavenumber space, $k$, slower than $\mathrm{e}^{-k/k_d}$ for some constant $k_d$), then our analysis is not relevant since a singularity is likely to form almost immediately. In such cases the presence of regularizing effects, such as viscosity, will play a crucial rôle in determining the motion.

### 1.3. *Outline of methodology*

In his original analysis, Moore (1979) solved the Birkhoff–Rott equation in terms of the natural independent variables, i.e. the (real) circulation, $\Gamma$, and the time, $t$. However, an alternative approach is to continue analytically the solution into the complex $\Gamma$-plane, identify key aspects of the analysis away from the real axis, and then to continue analytically the solution back to the real axis (Moore 1985; Caflisch & Orellana 1986). While this procedure may seem a little exotic, one of its advantages is that it provides a convenient way of analysing the nonlinearity that is often central to singularity formation. Indeed, the fact that nonlinear effects can be crucial follows from the observation that, in the case of a small sinusoidal perturbation, the solution to the linearized Birkhoff–Rott equation exists for all time.

Moreover, an approach based on analytic continuation into the complex plane has yielded important results in the past. For instance, using Moore's (1985) approximate differential equations, Caflisch & Orellana (1986) proved existence almost up to the time of singularity formation for initial data close to those of a flat sheet, while Duchon & Robert (1988) and Caflisch & Orellana (1989) have constructed exact solutions

† Surface tension (e.g. Pullin 1982; Baker & Nachbin 1998) is a less effective regularization because singularities can still develop as a result of the self-intersection of the interface (Hou, Lowengrub & Shelley 1997).

to the Birkhoff–Rott equation which display singularity formation in physical space. Also, by using an alternative nonlinear approximation to the Birkhoff–Rott equation, Caflisch & Semmes (1990) described singularity formation on a vortex sheet up to and including the time at which the physical singularity forms.

One of the conclusions of this earlier work (see also § 5), is that there is a family of possible physical singularities. The question then arises of which ones are likely to be observed in practice. By extending into the complex plane for early times, we show that for a wide class of initial conditions, nonlinear effects ensure that at times $t = 0+$, the analytically-continued curvature develops singularities proportional to $(\Gamma - \Gamma_s)^{-1/2}$, where $\Gamma_s(t)$ is the position of a singularity in the complex plane. As time evolves such singularities move around the complex plane. The first time at which a singularity intersects the real $\Gamma$-axis gives the time at which a singularity forms in the physical problem. We argue that the formation of these $(\Gamma - \Gamma_s)^{-1/2}$ curvature singularities at $t = 0+$ in the complex plane is in some sense generic, and explains why such singularities proportional to $|\Gamma - \Gamma_s|^{-1/2}$ are observed in the physical problem at later times.

A key feature in our analysis is that even if the initial disturbance is very small in physical space, then there are regions in the complex plane where the solution is nonlinear even at $t = 0+$. As a result of this observation, we are able to construct a self-consistent asymptotic solution to the problem that Moore (1979, 1985) studied, i.e. the evolution of an initially small sinusoid. Certain parts of our analysis are simply a re-expression of Moore's (1979, 1985) solution in a slightly more formal asymptotic language. However, we are also able to (*a*) identify where the $\frac{3}{2}$-power singularities originate from, (*b*) obtain an asymptotic description of the shape of the sheet as the singularity forms, and (*c*) suggest an explanation of certain results observed numerically for larger initial amplitudes. We note that the existence of a self-consistent asymptotic solution to Moore's (1979) problem is not surprising since the amplitude of the disturbance is still small at the moment that the singularity forms (cf. the rising Boussinesq bubble, etc.).

### 1.4. *Outline of the paper*

In § 2 we formulate the problem in the complex plane. Using a combined asymptotic and numerical argument, we show that for a wide range of initial conditions, singularities can develop at $t = 0+$; these singularities are consistent with the curvature singularity that Moore (1979) predicted would form on the real axis at a later time. Indeed, as time evolves the singularities that develop at $t = 0+$ move around the complex plane and may intersect the real axis. In § 3 we show that this picture is consistent with numerical solutions of the Birkhoff–Rott equation.

In § 4 we find an asymptotic solution to the problem where the initial disturbance is a small sinusoid. For $t = O(1)$ the analysis is based on an observation in § 2 that Moore's (1985) equations are *asymptotic* approximations far from the real $\Gamma$-axis. We follow previous authors and assume that the initial condition is antisymmetric about $\Gamma = 0$. A consequence of this simplification is that key features of the solution in the complex $\Gamma$-plane can be obtained by studying the real hyperbolic equations that apply on the imaginary $\Gamma$-axis (Moore 1985). These hyperbolic equations are solved both numerically and analytically. In particular, by means of a Hodograph transformation (Professor D. W. Moore and Professor J. T. Stuart, private communication), an expression is obtained for the long-time behaviour of the 'over-turning' singularity. However, solutions to these hyperbolic equations are only asymptotic approximations to the full problem while the singularity is far from the real $\Gamma$-axis. At times when

this condition is violated a different asymptotic approximation is necessary. At such times we find that the appropriate rescaling of the Birkhoff–Rott equation leads to a linearized problem, the solution of which specifies the shape of the vortex sheet at times close to singularity formation.

Finally, in § 5 we show that even if the vortex sheet has been deformed nonlinearly, at times close to the formation of a physical singularity, the shape of the sheet in the neighbourhood of the singularity is described by a linear equation. As a result it is possible to predict certain properties of singularity formation even when the initial perturbation is not small. This enables us to propose an alternative explanation of the observations that led Shelley (1992) to suggest that there might be a change in nature of the singularity when there is a large deformation of the vortex sheet.

## 2. Formulation and early-time singularity formation

### 2.1. *Formulation*

The evolution of a two-dimensional vortex sheet is described by the Birkhoff–Rott integro-differential equation (e.g. Birkhoff 1962)

$$\frac{\partial \overline{z(\xi,t)}}{\partial t} = \frac{1}{2\pi \mathrm{i}} \int_{-\infty}^{\infty} \frac{\Gamma_{\xi}(\hat{\xi})\,\mathrm{d}\hat{\xi}}{z(\xi,t) - z(\hat{\xi},t)}\,, \tag{2.1}$$

where the overbar denotes a complex conjugate, the integral is a Cauchy principal value, $\xi$ is a Lagrangian marker variable, $t$ is time, $z(\xi,t) = x(\xi,t) + \mathrm{i}y(\xi,t)$ is a complex coordinate giving the position of the vortex sheet, and $\Gamma(\xi)$ is the circulation in the sheet measured between the point with coordinate $z$ and a reference particle. For the most part, a subscript that is a variable will refer to differentiation with respect to that variable, e.g. $\Gamma_{\xi}(\xi) = \mathrm{d}\Gamma/\mathrm{d}\xi$. The independence of $\Gamma$ of time (due to Kelvin's circulation theorem) means that, if appropriate, the Birkhoff–Rott equation can be rewritten so that $\Gamma$ is the independent variable.

Except where stated otherwise, we will assume for simplicity that the sheet is $2\pi$-periodic, i.e. that $z(\xi + 2\pi, t) = 2\pi + z(\xi,t)$. This condition can for the most part be relaxed. For instance the analysis follows through for a disturbance to a uniform sheet that is non-periodic but decays sufficiently fast as $|\xi| \to \infty$; however, this generalization is at the expense of slightly more complicated algebra.

The choice of period sets the length scale of the motion. Further, for the motion of the sheet to be periodic, the vortex-sheet strength must also be $2\pi$-periodic. If we normalize the flow so that the average jump in the tangential velocity across the vortex sheet is unity, then this implies that $\Gamma(\xi + 2\pi) = 2\pi + \Gamma(\xi)$. Given these periodicity properties, (2.1) can be rewritten as

$$\frac{\partial \overline{z(\xi,t)}}{\partial t} = \frac{1}{4\pi \mathrm{i}} \int_{0}^{2\pi} \Gamma_{\xi}(\hat{\xi}) \cot\left(\tfrac{1}{2}(z(\xi,t) - z(\hat{\xi},t))\right)\,\mathrm{d}\hat{\xi}\,. \tag{2.2}$$

We wish to study the solution to (2.2) in the complex $\xi$-plane. To this end it is helpful to write the Cauchy principal value as a contour integral:

$$\int_{0}^{2\pi} \Gamma_{\xi}(\hat{\xi}) \cot\left(\tfrac{1}{2}(z(\xi,t) - z(\hat{\xi},t))\right)\mathrm{d}\hat{\xi} = \int_{\mathscr{C}} \Gamma_{\xi}(\hat{\xi}) \cot\left(\tfrac{1}{2}(z(\xi,t) - z(\hat{\xi},t))\right)\mathrm{d}\hat{\xi} + \frac{2\pi \mathrm{i}\Gamma_{\xi}(\xi)}{z_{\xi}(\xi,t)}\,, \tag{2.3}$$

where the contour $\mathscr{C}$ runs from $\hat{\xi} = 0$ to $\hat{\xi} = 2\pi$, and is assumed to be deformed

beneath a simple pole at $\hat{\xi} = \xi$. It is convenient to write

$$z(\xi, t) = \xi + s(\xi, t)\,, \quad \Gamma(\xi) = \xi + \sigma(\xi)\,, \tag{2.4}$$

so that the $2\pi$-periodic parts of $z$ and $\Gamma$ are identified as $s$ and $\sigma$ respectively. Following Caflisch & Orellana (1986), we introduce the $^*$ operator defined by

$$s^*(\xi, t) = \overline{s(\bar{\xi}, t)}\,. \tag{2.5}$$

With this definition, $s^*(\xi, t)$ is an analytic function of $\xi$ if, and only if, $s(\xi, t)$ is an analytic function of $\xi$. Further: ($a$) if $s$ and $s^*$ are known in the upper half-$\xi$-plane, then $s$ is known in the whole $\xi$-plane, ($b$) if $s$ is real when $\xi$ is real, then $s^* = s$ for all $\xi$, and ($c$) when $\xi$ is real, then $s^*(\xi, t) = \overline{s(\xi, t)}$. The last property means that the Birkhoff–Rott equation (2.2) can be analytically continued into the upper half complex-$\xi$-plane as

$$\frac{\partial s^*(\xi, t)}{\partial t} = \frac{1}{4\pi \mathrm{i}} \int_{\mathscr{C}} (1 + \sigma_{\hat{\xi}}(\hat{\xi})) \cot\left(\tfrac{1}{2} W(\xi, \hat{\xi}, t)\right) \mathrm{d}\hat{\xi} + \frac{(1 + \sigma_\xi(\xi))}{2(1 + s_\xi(\xi, t))}\,, \tag{2.6a}$$

where

$$W(\xi, \hat{\xi}, t) = \xi - \hat{\xi} + s(\xi, t) - s(\hat{\xi}, t)\,. \tag{2.6b}$$

Just how far into the upper half-plane we can extend the equation depends on the analytic properties of the integral in (2.6$a$). As $\mathrm{Im}(\xi)$ increases these properties depend both on whether $W$ is analytic on the integration contour and on whether $W$ is zero at some point on the contour (since if $W = 0$ at some point, then account must be taken of the contribution from the pole as it crosses the contour). For simplicity we will restrict attention to those points of the complex $\xi$-plane such that, as $\xi$ varies, the contour can be deformed both so that $W \neq 0$ on the contour and so that $W$ is analytic on the contour. Also, unless stated otherwise, and in order to fix ideas, we shall take the contour to run from $\hat{\xi} = 0$ to $\hat{\xi} = 2\pi$ along the real $\hat{\xi}$-axis. The region of analytic continuation will then be assumed to extend far enough into the upper half-plane for our purposes; we will rely on subsequent analysis and numerical calculations to confirm this assumption *a posteriori*.

We next rewrite (2.6$a$) in the alternative form

$$\frac{\partial s^*}{\partial t} = \frac{\sigma_\xi - s_\xi}{2(1 + s_\xi)} + J(\xi, t)\,, \tag{2.7a}$$

where

$$J(\xi, t) = \frac{1}{4\pi \mathrm{i}} \int_{\mathscr{C}} (1 + \sigma_{\hat{\xi}}(\hat{\xi})) \left(\mathrm{i} + \cot\left(\tfrac{1}{2} W(\xi, \hat{\xi}, t)\right)\right) \mathrm{d}\hat{\xi}\,. \tag{2.7b}$$

Similarly it follows from taking the complex conjugate of (2.2) before analytically continuing into the complex plane, that

$$\frac{\partial s}{\partial t} = -\frac{\sigma_\xi - s^*_\xi}{2(1 + s^*_\xi)} + K(\xi, t)\,, \tag{2.8a}$$

where

$$K(\xi, t) = -\frac{1}{4\pi \mathrm{i}} \int_{\mathscr{C}} (1 + \sigma_{\hat{\xi}}(\hat{\xi})) \left(\mathrm{i} + \cot\left(\tfrac{1}{2} W^*(\xi, \hat{\xi}, t)\right)\right) \mathrm{d}\hat{\xi} = J^*(\xi, t) - 1\,. \tag{2.8b}$$

Equations (2.7) and (2.8) highlight the significance of points $\xi = \xi_d(t)$ (if they exist) where either one, or both, of the conditions

$$1 + s_\xi(\xi_d, t) = 0 \quad \text{and} \quad 1 + s^*_\xi(\xi_d, t) = 0 \tag{2.9}$$

hold – points that we shall see are important in the formation of singularities in the upper half complex $\xi$-plane (singularity formation in the lower half-$\xi$-plane follows from the definition of $s^*$ above). However, before we employ (2.7) and (2.8) to such ends (see §§ 2.4–2.5), we note that another advantage of this form of the equations is that it is possible to obtain bounds on $J(\xi,t)$ and $K(\xi,t)$ when $\mathrm{Im}(\xi) \gg 1$. Therefore, we first digress in order to derive an asymptotic approximation of (2.7) and (2.8) that is valid when $\mathrm{Im}(\xi) \gg 1$. This approximation will be used both to study singularity formation for the initial condition used by MBO (§ 2.3), and to find an asymptotic solution valid for small-amplitude disturbances (§ 4.1).

### 2.2. *Simplified equations far from the real $\xi$-axis*

In order to estimate the magnitude of $J$ and $K$ when $\mathrm{Im}(\xi) \gg 1$, we need to understand the behaviour of $W = W_\mathrm{r} + \mathrm{i}W_\mathrm{i}$, and thence $\cot(\frac{1}{2}W)$, for $\mathrm{Im}(\xi) \gg 1$. From (2.6*b*), it is tempting to conclude that $W_\mathrm{i} \gg 1$ when $\mathrm{Im}(\xi) \gg 1$ (and similarly for $W^*$). This is desirable since then

$$\left|\mathrm{i} + \cot\left(\tfrac{1}{2}W\right)\right| \sim 2\exp(-W_\mathrm{i}) \ll 1\,, \tag{2.10a}$$

and

$$\left|\mathrm{i} + \cot\left(\tfrac{1}{2}W^*\right)\right| \sim 2\exp(-W_\mathrm{i}^*) \ll 1\,. \tag{2.10b}$$

However this need not be the case if $s(\xi,t)$ (or $s^*(\xi,t)$) grows faster than $\xi$ as $\mathrm{Im}(\xi) \to \infty$. For instance, in the case of the initial condition $s(\xi,0) = \epsilon\kappa\sin\xi$ (see (2.21)), there will be a range of $\mathrm{Re}(\xi)$ where for all fixed $\hat{\xi}$ on the contour $\mathscr{C}$, $W_\mathrm{i} \to -\infty$ as $\mathrm{Im}(\xi) \to \infty$. (This is of course not to say that for fixed large $\mathrm{Im}(\xi)$ it may not be possible to deform the contour so that $W_\mathrm{i} \gg 1$.)

For the purposes of § 2.3 and § 4.1 it is sufficient to note that in regions of the complex plane where

$$\mathrm{Im}(\xi) \gg 1\,, \quad s(\xi,t) = O(1) \quad \text{and} \quad s^*(\xi,t) = O(1)\,, \tag{2.11}$$

a straightforward estimate using (2.10) shows that for an integration contour $\mathscr{C}$ along the real $\hat{\xi}$-axis,

$$J = O(\exp(-\mathrm{Im}(\xi))) \quad \text{and} \quad K = O(\exp(-\mathrm{Im}(\xi)))\,. \tag{2.12}$$

In deriving (2.12) we have also assumed that $s(\hat{\xi},t) = O(1)$ and $s^*(\hat{\xi},t) = O(1)$ on $\mathscr{C}$, but this is not restrictive. Regions satisfying (2.11) arise in § 2.3 essentially because $s(\xi,0) = s^*(\xi,0) = 0$, and in § 4.1 because of the smallness of the initial amplitude $\epsilon$.

When condition (2.11) is satisfied, we conclude that a consistent leading-order asymptotic approximation to the Birkhoff–Rott equation is

$$\frac{\partial s^*}{\partial t} = \frac{\sigma_\xi - s_\xi}{2(1+s_\xi)}\,, \quad \frac{\partial s}{\partial t} = -\frac{\sigma_\xi - s_\xi^*}{2(1+s_\xi^*)}\,, \tag{2.13}$$

where $s$ and $s^*$ are functions of $\xi$ and $t$. We note that this asymptotic approximation can also be derived when the vortex sheet is not $2\pi$-periodic, but that under condition (2.11) the asymptotic error is then $O(1/\mathrm{Im}(\xi))$, rather than the error of $O(\exp(-\mathrm{Im}(\xi)))$ that follows from (2.12).

Caflisch & Orellana (1986) and Caflisch, Orellana & Siegel (1990) have previously derived equivalent equations by employing the upper, $s_+$, and lower, $s_-$, analytic components of $s$ ($s \sim s_-$ for $\mathrm{Im}(\xi) \gg 1$). An advantage of the present approach is that it is evident that (2.13) is an *asymptotic* approximation in those parts of the

complex plane where $\mathrm{Im}(\xi) \gg 1$ and $s(\xi, t) = O(1)$. In particular, we note that the approximation remains asymptotic for $\xi$ close to points $\xi_d(t)$ satisfying one or both the conditions (2.9).

### 2.3. *An example of a small-time solution*

For the rest of this section we will concentrate on understanding how singularities can develop in the solution even when the initial condition is entire (i.e. analytic in the whole complex $\xi$-plane). Moreover, we will not necessarily assume that the amplitude of the initial disturbance to the vortex sheet is small (cf. Moore 1979, 1985; § 4), instead we will seek early-time solutions, and use $t$ as our small asymptotic parameter.

We start by considering the MBO initial condition

$$s(\xi, 0) = 0, \quad \sigma_\xi(\xi) = \epsilon \cos(\xi), \tag{2.14}$$

and try to determine how singularities develop in $s$. As MBO show, this initial condition has certain simplifying properties which enable many terms of a power series solution in time to be calculated, the first two of which are

$$s = \tfrac{1}{2}\mathrm{i}\epsilon\, t \sin\xi - \tfrac{1}{8}\epsilon\, t^2 \sin\xi\,(1 + \epsilon\cos\xi) + \ldots . \tag{2.15}$$

However, no matter how small the time, $t \ll 1$, this power series does not converge far from the real $\xi$-axis. In particular, it follows from (2.15) that the series becomes disordered when

$$\exp(-\mathrm{i}\xi) \sim \epsilon^{-1} t^{-1}. \tag{2.16}$$

The nature of condition (2.16) suggests that for small times, and far from the real $\xi$-axis, a similarity solution should be sought of the form

$$\eta = \epsilon t \exp(-\mathrm{i}\xi)\,, \quad s = s_0(\eta) + O(t)\,, \quad s^* = s_0^*(\eta) + O(t)\,, \tag{2.17}$$

where the region of the complex $\xi$-plane of interest is that where $\mathrm{Im}(\xi) \approx -\ln(\epsilon t) \gg 1$. Since $s$, $s^* = O(1)$ in scaling (2.17), condition (2.11) is satisfied. Hence, from (2.13), (2.14) and (2.17), we find that to leading order

$$s_{0\eta} = -\frac{1}{4(1 - \mathrm{i}\eta s_{0\eta}^*)}\,, \qquad s_{0\eta}^* = \frac{1}{4(1 - \mathrm{i}\eta s_{0\eta})}\,. \tag{2.18}$$

The solution to (2.18) which matches with (2.15) as $\eta \to 0$ is

$$s_{0\eta} = \frac{2 - \mathrm{i}\eta - (4 - \eta^2)^{1/2}}{4\mathrm{i}\eta}\,, \quad s_{0\eta}^* = \frac{2 + \mathrm{i}\eta - (4 - \eta^2)^{1/2}}{4\mathrm{i}\eta}\,. \tag{2.19}$$

In order to fix the discussion, we assume that $-\pi/2 < \mathrm{Re}(\xi) < \pi/2$; then $\mathrm{Im}(\xi) > 0$ corresponds to $\mathrm{Re}(\eta) > 0$. It follows from (2.19) that both $s_{0\eta}$ and $s_{0\eta}^*$ have square-root singularities at $\eta = 2$. In other words, for $t \ll 1$ we have shown that $s$ and $s^*$ have $\frac{3}{2}$-power singularities at

$$\xi \sim \mathrm{i}\ln\left(\frac{2}{\epsilon t}\right)\,. \tag{2.20}$$

Thus these singularities propagate in from infinity toward the real $\xi$-axis. They have the same exponent (i.e. a square-root singularity in $s_\xi$) as the singularity that develops at a later time on the real axis (MBO). We argue in § 2.5 that this is no coincidence.

### 2.4. *A class of small-time solutions*

While the initial condition (2.14) has been used in several numerical calculations (MBO; Shelley 1992), general conclusions cannot be drawn from the above analysis. One way forward might be to generalize (2.14) to a family of initial conditions for which singularities propagate in from infinity. Instead we will consider the class of initial conditions such that at $t = 0$ there exists at least one finite point, $\xi_0 = \xi_d(0)$, satisfying either one or both of the conditions (2.9). This class includes the initial condition

$$s = \epsilon\kappa \sin(\xi)\,, \quad \sigma = 0\,, \tag{2.21}$$

used by Moore (1979) and Krasny (1986*a*), who took $\kappa = \mathrm{i}$ and $\kappa = (\mathrm{i} - 1)$ respectively.†

For $t \ll 1$ a series solution to (2.7) and (2.8) can be found of the form

$$s = s_0(\xi) + ts_1(\xi) + \dots\,, \quad s^* = s_0^*(\xi) + ts_1^*(\xi) + \dots\,, \tag{2.22}$$

where

$$s_0(\xi) = s(\xi, 0)\,, \quad s_1(\xi) = -\frac{\sigma_\xi - s_{0\xi}^*}{2(1 + s_{0\xi}^*)} + K(\xi, 0)\,, \tag{2.23}$$

and

$$s_0^*(\xi) = s^*(\xi, 0)\,, \quad s_1^*(\xi) = \frac{\sigma_\xi - s_{0\xi}}{2(1 + s_{0\xi})} + J(\xi, 0)\,. \tag{2.24}$$

However, this series solution is not uniformly valid. In particular it breaks down near points where $(1 + s_{0\xi}) = 0$ and/or $(1 + s_{0\xi}^*) = 0$. We consider two cases in detail. First in § 2.4.1 we examine the solution near a point $\xi = \xi_0$ where $(1 + s_{0\xi}) = 0$ but $(1 + s_{0\xi}^*) \neq 0$ (the case where $(1 + s_{0\xi}^*) = 0$ but $(1 + s_{0\xi}) \neq 0$ is very similar and will not be discussed separately). Subsequently in § 2.4.2 we assume that both $(1 + s_{0\xi})$ and $(1 + s_{0\xi}^*)$ are zero simultaneously at $\xi = \xi_0$.

#### 2.4.1. *The case* $(1 + s_{0\xi}(\xi_0)) = 0$ *and* $(1 + s_{0\xi}^*(\xi_0)) \neq 0$.

Near $\xi = \xi_0$ it is necessary to introduce a rescaling. In order to determine the appropriate asymptotic structure, we first expand the solution (2.22) as a power series in $\zeta = \xi - \xi_0$:

$$s = s_{00} - \zeta + \tfrac{1}{2}s_{02}\zeta^2 + \dots + \left(\frac{s_{01}^* - \sigma_{01}}{2(1 + s_{01}^*)} + K_{00} + \dots\right) t + \dots\,, \tag{2.25a}$$

$$s^* = s_{00}^* + s_{01}^*\zeta + \tfrac{1}{2}s_{02}^*\zeta^2 + \dots + \left(\frac{1 + \sigma_{01}}{2s_{02}\zeta} + \dots\right) t + \dots\,, \tag{2.25b}$$

where

$$s_{0n} = \frac{\partial^n s_0}{\partial \xi^n}(\xi_0)\,, \quad \sigma_{01} = \sigma_\xi(\xi_0)\,, \quad \text{and} \quad K_{00} = K(\xi_0, 0)\,. \tag{2.25c}$$

The non-uniformity arises from the leading coefficient of the $O(t)$ term in (2.25*b*). Further, from the coupled nature of (2.7) and (2.8), we expect that the leading coefficient of the $O(t)$ term in (2.25*a*) will play a determining rôle in the asymptotic structure. This indicates that the key terms are those including $s_{01}^*$ and $s_{02}$. These terms are comparable in (2.25) when $\zeta = O(t^{1/2})$; this in turn suggests that the appropriate

† Actually, Krasny (1986*a*) used $\kappa = 1 - \mathrm{i}$, but we have shifted his profile through half a wavelength to simplify comparison with Moore's initial profile.

asymptotic scaling for small $\zeta$ when $t \ll 1$ is

$$\zeta = \eta\omega t^{1/2} \quad \text{where} \quad \omega = \left(\frac{2(1+\sigma_{01})}{s_{02}(1+s_{01}^*)}\right)^{1/2} . \tag{2.26}$$

In order to match with the series (2.25), $s$ and $s^*$ need to be expanded as

$$s = s_{00} - \eta\omega t^{1/2} + \left(\tfrac{1}{2} + J_{00}^* + \frac{1+\sigma_{01}}{(1+s_{01}^*)}A(\eta)\right) t + \dots , \tag{2.27a}$$

$$s^* = s_{00}^* + \left((1+s_{01}^*)B(\eta) - \eta\right)\omega t^{1/2} + \dots . \tag{2.27b}$$

It then follows from substituting (2.26) and (2.27) into (2.7) and (2.8) that

$$2A - \eta A_\eta = -\frac{1}{B_\eta} , \quad B - \eta B_\eta = \frac{1}{A_\eta} . \tag{2.28}$$

If the solution (2.27) is to match with (2.25), then we require that $A \to \eta^2 - 1/2$ and $B \to \eta$ as $\eta \to \infty$. For the purposes of the subsequent numerical solution, we note that further terms of this asymptotic boundary condition are straightforward to find; for instance, correct to $O(\eta^{-10})$:

$$A = \eta^2 - \frac{1}{2} - \frac{1}{16\eta^2} - \frac{1}{96\eta^4} + \frac{1}{768\eta^6} + \frac{7}{3840\eta^8} + O\left(\frac{1}{\eta^{10}}\right) , \tag{2.29a}$$

$$B = \eta + \frac{1}{4\eta} - \frac{1}{192\eta^5} - \frac{1}{768\eta^7} + \frac{1}{2560\eta^9} + O\left(\frac{1}{\eta^{11}}\right) . \tag{2.29b}$$

The system (2.28) and (2.29) has no free parameters; as such it is sufficient to determine $A$ and $B$ uniquely. While we have been unable to find an analytic solution, it is quite straightforward to construct a numerical one. Moreover, because it follows from (2.28) and (2.29) that $A(\overline{\eta}) = \overline{A(\eta)}$, $B(\overline{\eta}) = \overline{B(\eta)}$, and $A(-\eta) = A(\eta)$, $B(-\eta) = -B(\eta)$, the numerical solution need only be found in one quadrant.

For our numerical calculations we found it convenient to differentiate (2.28) to obtain a first-order system for the unknowns $A_\eta$ and $B_\eta$:

$$A_{\eta\eta} = \frac{\eta A_\eta^3 B_\eta^2}{1+\eta^2 A_\eta^2 B_\eta^2} , \quad B_{\eta\eta} = \frac{A_\eta B_\eta^2}{1+\eta^2 A_\eta^2 B_\eta^2} . \tag{2.30}$$

This system was integrated using a standard fourth-order Runge–Kutta method. As an accuracy check we calculated the solution at the origin by integrating in along the real axis from $\eta = L + \mathrm{i}0$, using (2.29) as the initial condition. We confirmed that the error in the solution could be reduced to little more than rounding error by taking $L$ sufficiently large and by the choice of a sufficiently small step size in the Runge–Kutta method. Accuracy tests were also performed by integrating to the origin along the imaginary axis from $\eta = 0 + \mathrm{i}L$.

From examining the calculated solution for $A_\eta$ and $B_\eta$, we found no singularities along the real or imaginary axis of $\eta$. Yet the results at the origin were different, implying the presence of one or more singularities somewhere in the first quadrant. In order to help determine the nature of such singularities, the integrals

$$I_1(A) = \frac{\mathrm{i}}{2\pi}\oint_{\mathscr{D}} \frac{A_{\eta\eta\eta}}{A_{\eta\eta}}\mathrm{d}\eta \qquad \text{and} \qquad I_2(A) = \frac{\mathrm{i}}{2\pi}\oint_{\mathscr{D}} \frac{\eta A_{\eta\eta\eta}}{A_{\eta\eta}}\mathrm{d}\eta , \tag{2.31}$$

were evaluated for various closed contours, where the contour $\mathscr{D}$ was traversed twice.

If $A$ has a $\frac{3}{2}$-power singularity at $\eta = \eta_0$, and if $\mathscr{D}$ encloses $\eta_0$ but no other singularity (e.g. if it is sufficiently close to $\eta_0$), then it can be shown that

$$I_1(A) = 1 \qquad \text{and} \qquad I_2(A) = \eta_0 \,. \tag{2.32}$$

A search of the first quadrant using various circular and rectangular contours yielded a singularity at

$$\eta_0 \approx 0.7359 + \mathrm{i}0.4920 \,. \tag{2.33}$$

While we quote the result to four significant digits, sensitivity tests based on varying the step size, etc., suggested that our calculations were accurate to about $\pm 10^{-8}(1 \pm \mathrm{i})$. Further, the integral $I_2(B)$ indicated that, to within our error estimate, there was a singularity in $B$ at the same location. We found no other singularities in the first quadrant for those cases when we initiated our numerical calculations at some place far from the origin in the first quadrant. We shall refer to the singularity at (2.33) and its mirror images in the other three quadrants as the primary singularities. Of the singularities close to $\xi_0$, it is one (or more) of these singularities that are on the same Riemann sheet as the real physical axis, and lie closest to the real physical axis.

However, the primary singularities are not the only singularities in the solution to (2.30). Other singularities were found on the different Riemann sheets associated with the primary singularities. For instance, by integrating from infinity along the negative imaginary axis and then proceeding into the first quadrant, another singularity was found at $0.0829 + \mathrm{i}0.1240$. We also found its symmetric counterpart in the second quadrant on the same Riemann sheet. To find the symmetric counterparts in the third and fourth quadrants it is necessary to integrate from infinity along the positive imaginary axis. We have not tried to find any other singularities, because it is only the primary singularities that are of consequence in our study.

The singularities we found were all deduced to be $\frac{3}{2}$-power singularities, both from the behaviour of the solutions and the consistent values of $I_1(A)$ and $I_1(B)$ for different contours. In particular, (*a*) the solution always returns to its initial value, within the accuracy of the calculation, after two circuits around a singularity, and (*b*) the integrals $I_1$ always evaluated to 1 within an accuracy of $10^{-9}$.

Moreover, such singularities are admitted by (2.28). For suppose that for $|\eta - \eta_0| \ll 1$, $A$ and $B$ expand as

$$A = A_0 + A_1(\eta - \eta_0) + A_p(\eta - \eta_0)^p + \dots \,, \tag{2.34a}$$

$$B = B_0 + B_1(\eta - \eta_0) + B_p(\eta - \eta_0)^p + \dots \,, \tag{2.34b}$$

where the $A_j$ and $B_j$ are constants, and $1 < p < 2$. Then the expansions (2.34) are solutions to (2.28) if certain consistency conditions are satisfied. For the coefficients given in (2.34), these conditions are $A_1 B_1 \neq 0$ and

$$\eta_0^2 = -\frac{1}{A_1^2 B_1^2} \neq 0\,, \quad 2A_0 = \eta_0 A_1 - \frac{1}{B_1}\,, \quad B_0 = \eta_0 B_1 + \frac{1}{A_1}\,, \quad A_p = \eta_0 A_1^2 B_p\,. \tag{2.35}$$

Our numerical solution shows that $p = \frac{3}{2}$ is selected. We note that this choice leads to the least number of terms in the power series expansion (2.34) when nonlinear interactions are taken into account.

2.4.2. *The case* $(1 + s_{0\xi}(\xi_0)) = 0$ *and* $(1 + s^*_{0\xi}(\xi_0)) = 0$.

The above analysis is not valid if $(1 + s_{0\xi})$ and $(1 + s^*_{0\xi})$ are simultaneously zero, e.g. if $\kappa$ in (2.21) is real. In this case, the series solution (2.22) becomes disordered in the neighbourhood of $\xi = \xi_0$ when $\zeta = O(t^{1/3})$. As a result, the scaling (2.26) and the

expansions (2.27) need to be replaced by

$$\zeta = \eta\Omega t^{1/3}\,, \quad \Omega = \left(\frac{4(1+\sigma_{01})}{s_{02}s_{02}^*}\right)^{1/3}\,, \tag{2.36}$$

and

$$s = s_{00} - \eta\Omega t^{1/3} + \tfrac{1}{2}s_{02}\Omega^2 A(\eta)t^{2/3} + \dots\,, \tag{2.37a}$$

$$s^* = s_{00}^* - \eta\Omega t^{1/3} + \tfrac{1}{2}s_{02}^*\Omega^2 B(\eta)t^{2/3} + \dots\,, \tag{2.37b}$$

respectively. The revised similarity equations for $A$ and $B$ are

$$2A - \eta A_\eta = -\frac{3}{2B_\eta}\,, \quad 2B - \eta B_\eta = \frac{3}{2A_\eta}\,, \tag{2.38}$$

with boundary conditions

$$A \to \eta^2 - \frac{1}{4\eta} + \dots\,, \quad B \to \eta^2 + \frac{1}{4\eta} + \dots \qquad \text{as} \qquad \eta \to \infty\,. \tag{2.39}$$

As before no analytical solution could be found. However, three symmetry conditions can be deduced from (2.38) and (2.39), namely (i) $A(\overline{\eta}) = \overline{A(\eta)}$, $B(\overline{\eta}) = \overline{B(\eta)}$, (ii) $A(-\eta) = B(\eta)$, $B(-\eta) = A(\eta)$, and (iii) $A(\mathrm{e}^{2\pi\mathrm{i}/3}\eta) = \mathrm{e}^{-2\pi\mathrm{i}/3}A(\eta)$, $B(\mathrm{e}^{2\pi\mathrm{i}/3}\eta) = \mathrm{e}^{-2\pi\mathrm{i}/3}B(\eta)$. Therefore the full solution can be constructed once a solution has been found in any sector of the complex plane of angle of $\pi/6$.

In order to locate the singularities of (2.38) the same procedure as for (2.28) was followed. First, (2.38) was differentiated to obtain a system of equations for $A_\eta$ and $B_\eta$. Next the far-field behaviour analogous to (2.29) was determined, and then we numerically integrated inwards using a fourth-order Runge–Kutta method. Using the integral diagnostics (2.32), we found a ring of six branch-point singularities of $\frac{3}{2}$-power located at

$$\eta_0^6 \approx -0.9685\,. \tag{2.40}$$

We believe that these are the primary singularities as far as the solution on the same Riemann sheet as the physical real axis is concerned. In this case a search was not made for singularities on the other Riemann sheets.

In order to confirm that a $\frac{3}{2}$-power singularity is feasible, we again note that equations (2.38) admit a singularity of the form (2.34) for $1 < p < 2$ if $A_1B_1 \neq 0$ and

$$\eta_0^2 = -\frac{9}{4A_1^2B_1^2} \neq 0\,, \quad A_0 = \tfrac{1}{2}\eta_0 A_1 - \frac{3}{4B_1}\,, \quad B_0 = \tfrac{1}{2}\eta_0 B_1 + \frac{3}{4A_1}\,, \quad 3A_p = 2\eta_0 A_1^2 B_p\,. \tag{2.41}$$

### 2.5. *Motion of the singularities*

In the previous two sub-sections we have shown that for a range of initial conditions, branch-point singularities of power $\frac{3}{2}$ appear spontaneously in the complex plane at time $t = 0+$. Since the singularities (2.33) and (2.40) are not at the origin of the $\eta$-plane, it follows from (2.26) and (2.36) respectively that the singularities move away from $\xi = \xi_0$ as time increases. In this sub-section we show that for times $t = O(1)$ the singularities can continue to move around the complex plane.

Suppose that at time $t$ a singularity is at $\xi = \xi_s(t)$. Close to the singularity seek an asymptotic expansion of the form

$$s = S_0(t) + S_1(t)\eta + S_p(t)\eta^p + \dots\,, \tag{2.42a}$$

$$s^* = S_0^*(t) + S_1^*(t)\eta + S_p^*(t)\eta^p + \dots\,, \tag{2.42b}$$

where we now define $\eta = \xi - \xi_s(t)$. On substituting (2.42) into (2.7) and (2.8), and equating like powers of $\eta$, we find that (2.42) is an acceptable local solution if certain consistency conditions are satisfied; for the functions specified in (2.42) these are

$$\dot{S}_0 - \dot{\xi}_s S_1 = -\frac{\mathscr{Q}_s - S_1^*}{2(1+S_1^*)} + K(\xi_s, t), \quad \dot{S}_0^* - \dot{\xi}_s S_1^* = \frac{\mathscr{Q}_s - S_1}{2(1+S_1)} + J(\xi_s, t), \tag{2.43a}$$

$$\dot{\xi}_s^2 = -\left(\frac{1+\mathscr{Q}_s}{2(1+S_1)(1+S_1^*)}\right)^2, \quad S_p = \frac{2(1+S_1)^2 S_p^*}{(1+\mathscr{Q}_s)}\dot{\xi}_s, \tag{2.43b}$$

where $\mathscr{Q}_s(t) = \sigma_\xi(\xi_s(t))$, and a 'dot' denotes differentiation with respect to time. For small times (2.42), subject to (2.43), can be shown to match with (2.34), subject to (2.35) or (2.41). We emphasize that this result holds for any fixed $p$ for $1 < p < 2$.

We conclude that $\frac{3}{2}$-power singularities generated spontaneously at $t = 0+$ can move round the plane at later times. Moreover, (2.42) and (2.43) indicate that the singularities will in general not change their power. A possible exception is when two singularities collide; however Caflisch *et al.* (1993) have predicted on theoretical grounds that both singularities remain intact after collision.

In the next section we will compute, *inter alia*, the motion of the singularities for Krasny's initial condition and demonstrate that for sufficiently small initial amplitudes a pair collides on the imaginary $\xi$-axis. After the collision, we detect a singularity of $\frac{3}{2}$-power approaching the real axis along the imaginary axis. However, what is more important is that a singularity can collide on the real $\xi$-axis with its symmetric counterpart from below the real axis. This event signals the occurrence of a $\frac{3}{2}$-power *physical* singularity. Previous numerical studies (Krasny 1986*a*; Shelley 1992) provide convincing evidence that $\frac{3}{2}$-power singularities reach the real $\xi$-axis in finite time. The above analysis indicates that such $\frac{3}{2}$-power singularities can arise for a wide range of initial conditions. We conclude that because such singularities can move around the complex plane without change of power, and in particular can reach the real $\xi$-axis in finite time, it is likely that Moore's physical singularity will also be observed for a wide range of initial conditions.

## 3. Numerical validation

The asymptotic results were confirmed by direct numerical solution of (2.2) using the spectrally accurate, alternate point trapezoidal rule (Baker 1983; Shelley 1992), and the spectral filtering technique introduced by Krasny (1986*a*). We used up to 512 points on the interface, with a time step of 0.001 in an Adams–Moulton fourth-order predictor-corrector, and with the filter level set to $10^{-25}$. The calculations were performed in double precision on a CRAY YMP.

We concentrate on the formation of singularities for the class of initial conditions (2.21). The asymptotic theory predicts the formation of singularities where one or more of the equations (2.9) is satisfied.

### 3.1. *Moore's initial condition*

For Moore's initial condition ($\kappa = \mathrm{i}$), singularities form at

$$\xi = \pm\frac{\pi}{2} \mp \mathrm{i}\left(\ln\left((1+\epsilon^2)^{1/2}+1\right) - \ln\epsilon\right) + 2m\pi \qquad (m = \ldots, -1, 0, 1, \ldots), \tag{3.1a}$$

corresponding to $1 + s_{0\xi} = 0$, and at

$$\xi = \pm\frac{\pi}{2} \pm \mathrm{i}\left(\ln\left((1+\epsilon^2)^{1/2}+1\right) - \ln\epsilon\right) + 2m\pi \qquad (m = \ldots, -1, 0, 1, \ldots), \tag{3.1b}$$

corresponding to $1 + s^*_{0\xi} = 0$.

Without loss of generality, we concentrate on the behaviour in one periodic window, $-\pi \leqslant \mathrm{Re}(\xi) \leqslant \pi$. According to (3.1), singularities form at $\xi_0$, $\bar{\xi}_0$, $-\xi_0$ and $-\bar{\xi}_0$, where

$$\xi_0 = \frac{\pi}{2} + \mathrm{i}\left(\ln\left((1+\epsilon^2)^{1/2}+1\right) - \ln\epsilon\right). \tag{3.2}$$

The symmetry in these positions reflects the symmetry in the initial condition. At each of these locations, a pattern of singularities is generated as described by (2.26), (2.27) (2.33) and (2.34). We are interested in those singularities that move towards the real axis, and in particular the one that is closest to the real axis. By evaluating (2.26) using (3.2) and the symmetry properties of $A$ and $B$, we can determine that the singularity in the vicinity of $\xi_0$ which is initially closest to the real axis is at

$$\xi \sim \xi_0 - \frac{\mathrm{e}^{\mathrm{i}\pi/4}}{(1+\epsilon^2)^{1/4}}\,\eta_0\, t^{1/2}, \tag{3.3}$$

where $\eta_0$ is given by (2.33). There is of course no guarantee that of the singularities initially formed at $\xi = \xi_0$ this is the singularity that remains closest to the real axis at later times. However, as indicated below, our numerical calculations suggest that it is. As a result of the top/down, left/right symmetry, there are similar singularities an identical distance from the real axis close to $\bar{\xi}_0$, $-\xi_0$ and $-\bar{\xi}_0$.

In order to make a comparison between the asymptotic prediction (3.3) and our numerical results, it is necessary to extract the position of the nearest singularity from the numerical solution. This can be done from the Fourier spectrum of $(z(\xi,t) - \xi)$, because the presence of a pair of branch-point singularities of power $(\nu + \mathrm{i}\mu)$ placed symmetrically on either side of the $\mathrm{Im}(\xi)$-axis, say at $\xi_s$ and $-\bar{\xi}_s$, means that the tail of the Fourier spectrum for large positive $k$ has the form

$$\frac{\mathrm{i}\mathscr{A}}{k^{1+\nu}}\,\exp(-\mathrm{Im}(\xi_s)k)\sin(\mathrm{Re}(\xi_s)k + \mu\ln k + \phi), \tag{3.4}$$

where $\mathscr{A}$ and $\phi$ are real constants (Carrier, Krook & Pearson 1966; Pugh 1989). A derivation of the equivalent formula for large negative $k$ is given in Appendix A (see (A 6)) as part of the asymptotic analysis needed for § 4.

Following previous work (Krasny 1986*a*; Pugh 1989; Shelley 1992; Baker *et al.* 1993), we form-fit the numerically generated spectrum for $(z(\xi,t) - \xi)$ to (3.4) for large, positive $k$. The procedure used was that of Baker *et al.* (1993), which is a refinement of Pugh's (1989) approach. As is usual the estimates for the position $\xi_s$ are better than for the power $(\nu + \mathrm{i}\mu)$. However, we find $\nu = 3/2$ and $\mu = 0$ correct to approximately one decimal place.

In figure 1, we show the trajectory of the singularity closest to the real axis both as predicted by the asymptotic formula (3.3) and as calculated numerically. Only the singularity in the strip $0 < \mathrm{Re}(\xi) < \pi/2$, $\mathrm{Im}(\xi) > 0$ is shown. The trajectory from the asymptotic theory, shown as a dashed line, is limited to the time interval $[0, t_1]$, where $t_1$ is the first time at which we can reliably detect the the presence of the singularity in the numerical results. Results for three different amplitudes $\epsilon$, as defined in (2.21), are illustrated.

In plot (*a*) the amplitude is $\epsilon = 0.5$. The singularity forms initially at $\pi/2 + \mathrm{i}1.444$, and we could first detect the presence of a singularity in the spectrum of the numerical

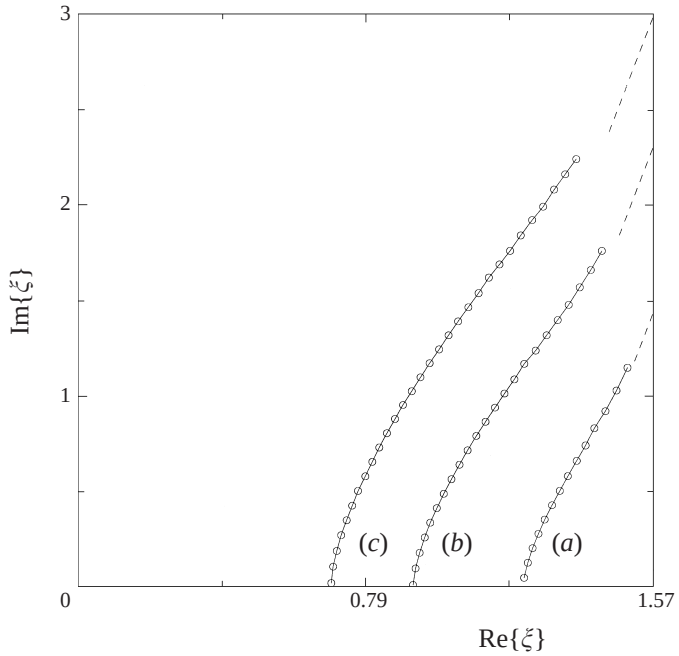


FIGURE 1. The motion of the $\frac{3}{2}$-singularity in the complex $\xi$-plane as determined by a form-fit to the Fourier spectra of the numerical solutions. Moore's initial condition is used and the location is shown as a sequence of circles connected by solid lines for three different initial amplitudes: (*a*) $\epsilon = 0.5$, (*b*) $\epsilon = 0.2$, (*c*) $\epsilon = 0.1$. Dashed lines show the corresponding motion as predicted by asymptotic formula (3.3) for small times.

results at $t_1 = 0.1$. The subsequent trajectory of the singularity is plotted as a sequence of connected circles spaced 0.1 units of time apart. The numerical result is in fairly good agreement with the asymptotic result at $t = t_1$ (i.e. the end of the dashed line).

In plot (*b*) we show results for $\epsilon = 0.2$. The singularity forms initially at $\pi/2 + \mathrm{i}2.312$, and we could first numerically detect the presence of the singularity at $t_1 = 0.3$. Again the agreement with the asymptotic prediction is reasonable, although it would no doubt improve if we could reliably extract the position of the singularity at even earlier times. However, when $\epsilon \ll 1$, the singularity is far from the real axis at small times, with the result that the exponential decay of the Fourier coefficients is very rapid. Consequently rounding error prevents there being any range of large $k$ over which a reliable numerical form-fit can be done.

The problem of obtaining reliable form fits for small times is even worse for the case $\epsilon = 0.1$ – see plot (*c*). The singularity that forms at $\pi/2 + \mathrm{i}2.998$ cannot be reliably detected until $t_1 = 0.5$. Consequently the agreement between the asymptotic theory and the numerical results is less good. Finally we note that if $\epsilon$ were small enough, then we would expect the singularity to collide with its mirror image on the imaginary axis before reaching the real axis at $\xi = 0$. This possibility is numerically confirmed for Krasny's initial condition below.

### 3.2. *Krasny's initial condition*

Krasny's initial condition corresponds to taking $\kappa = \mathrm{i} - 1$ in (2.21). The pattern in the singularities is then similar to that for Moore's initial condition. Again singularities initially form in the vicinity of four points, i.e. $\xi_0$, $-\xi_0$, $\bar{\xi}_0$ and $\bar{\xi}_0$, where in this case

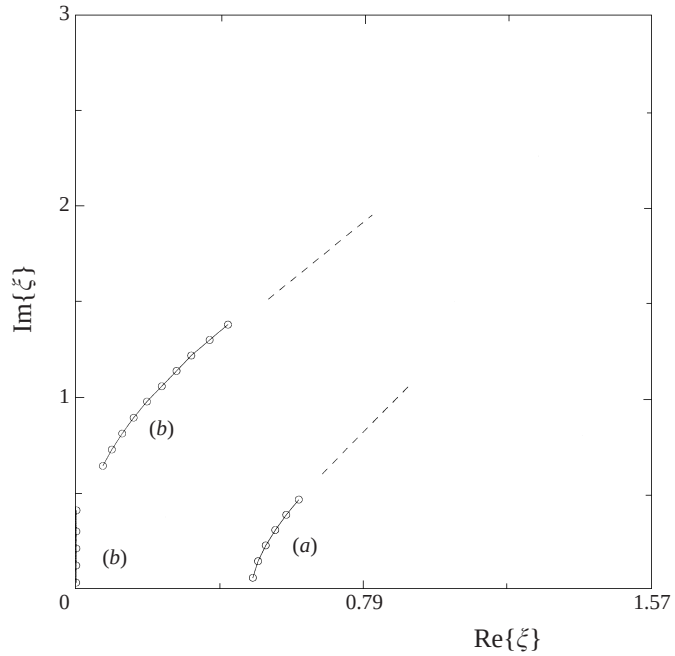


FIGURE 2. The same as figure 1, but for Krasny's initial condition with (*a*) $\epsilon = 0.5$, (*b*) $\epsilon = 0.2$.

(cf. (3.2))

$$\xi_0 = \mathrm{i} \ln \left( \frac{1 + (1 - 2\mathrm{i}\epsilon^2)^{1/2}}{(1 + \mathrm{i})\epsilon} \right) . \tag{3.5}$$

The trajectory of the singularity in the neighbourhood of $\xi_0$ that is closest to the real axis is given for small times from (2.26) and (3.5) as

$$\xi \sim \xi_0 - \left( \frac{2\mathrm{i}}{1 - 2\mathrm{i}\epsilon^2} \right)^{1/4} \eta_0 \, t^{1/2} . \tag{3.6}$$

We use the same procedure to form-fit the numerically generated spectrum. The results are again consistent with $\frac{3}{2}$-branch point singularities. Using the symmetry properties of the solution we restrict attention to the strip $0 < \mathrm{Re}(\xi) < \pi/2$, $\mathrm{Im}(\xi) > 0$. In figure 2 we show the trajectory of the singularity closest to the real axis for two representative cases that show different behaviour. Plot (*a*) is for an amplitude $\epsilon = 0.5$. The singularity forms at $0.9046 + \mathrm{i}1.0613$, and we can reliably detect its presence for $t > t_1 = 0.25$; its subsequent motion is shown as connected circles placed at intervals of 0.05 in time. The trajectory is similar to the ones illustrated in figure 1 in that it reaches the real axis at $\xi \neq 0$.

Plot (*b*) is for $\epsilon = 0.2$. The singularity forms at $0.8054 + \mathrm{i}1.9566$ and we can reliably locate it for $t_1 = 0.25 \leqslant t \leqslant 0.7$ and $t \geqslant 0.85$. For $0.7 < t < 0.85$ it is difficult to fit the spectrum to the form (3.4) because of the small value of $\mathrm{Re}(\xi_s)$; in particular we do not have a sufficiently large range in $k$ to detect accurately the gradual modulation in the spectrum due to the sine function. However, after the singularity collides with its mirror image when it reaches the imaginary axis, we can detect the singularity closest to the real axis and confirm that it reaches $\xi = 0$ after a finite time. These results are consistent with Krasny's (1986*a*) observations that for large enough initial amplitudes

the vortex sheet showed the formation of two symmetrically placed singularities, but that for small enough amplitudes, there was only one centrally placed singularity.

## 4. An asymptotic solution for initially small sinusoidal perturbations

In this section we obtain an asymptotic solution to the Birkhoff–Rott equation when the initial amplitude of the disturbance is small, i.e. $\epsilon \ll 1$. For definiteness we will concentrate on the cases where the solution is antisymmetric about, say, $\xi = 0$; this is the case for initial conditions (2.14) and (2.21). We believe that the analysis can be extended with slightly more effort to the general case provided that the initial amplitude is small.

### 4.1. *The solution far from the real axis*

Following earlier authors, we identify the Lagrangian coordinate $\xi$ with the circulation $\Gamma$, so that $\sigma(\xi) = 0$. The main advantage of this approach is that equations (2.13) then no longer have a variable coefficient $\sigma_\xi$ in them. The disadvantage is that the MBO initial condition (2.14) is given implicitly. The numerical results of § 3, in accordance with previous numerical results (Krasny 1986*a*; Shelley 1992), show that the singularities approach the real axis along the imaginary axis when the initial amplitude is sufficiently small. Therefore, following Moore (1985) and others, we consider the solution on the imaginary axis, $\xi = \mathrm{i}y$, and write $f(y,t) = s(\xi,t)$. As a consequence of the assumed antisymmetry, it follows that $f(-y,t) = -f(y,t)$ and $f^*(y,t) = -s^*(\xi,t)$.

In the case of sinusoidal perturbations that are small, the singularities initially form far from the real $\xi$-axis, i.e. in a region where (2.13) are leading-order asymptotic approximations of the Birkhoff–Rott equation. In terms of $f$ these equations become

$$f_t = \frac{\mathrm{i}f_y^*}{2(1+\mathrm{i}f_y^*)}, \quad f_t^* = -\frac{\mathrm{i}f_y}{2(1-\mathrm{i}f_y)}. \tag{4.1}$$

Following Moore (1985) this system can be further simplified by introducing the real functions $h(y,t)$ and $g(y,t)$ defined by

$$1-\mathrm{i}f_y = \left(\frac{h\mathrm{e}^{-\mathrm{i}g}}{2}\right)^{1/2}, \quad \text{or equivalently} \quad 1+\mathrm{i}f_y^* = \left(\frac{h\mathrm{e}^{\mathrm{i}g}}{2}\right)^{1/2}. \tag{4.2}$$

After differentiation with respect to $y$, system (4.1) becomes

$$h_t = g_y\,, \quad h^2 g_t = h_y\,. \tag{4.3}$$

We will focus on solutions to (4.3) with the initial conditions:

$$\text{MBO:}\ h = \frac{2}{(1+\epsilon\cosh\zeta)^2}, \quad g = 0, \quad \text{where} \quad y = \zeta + \epsilon\sinh\zeta\,; \tag{4.4a}$$

$$\text{Krasny:}\ h = 2\left(1 - 2\epsilon\cosh y + 2\epsilon^2\cosh^2 y\right), \quad g = -2\arctan\left(\frac{\epsilon\cosh y}{1-\epsilon\cosh y}\right); \tag{4.4b}$$

$$\text{Moore:}\ h = 2\left(1+\epsilon^2\cosh^2 y\right), \quad g = -2\arctan\left(\epsilon\cosh y\right). \tag{4.4c}$$

The derivation of (4.3) depends on the assumption that $y \gg 1$. This assumption can be made formal by writing

$$y = \ln(1/\epsilon) + Y, \quad \text{and} \quad \zeta = \ln(1/\epsilon) + \eta\,. \tag{4.5}$$

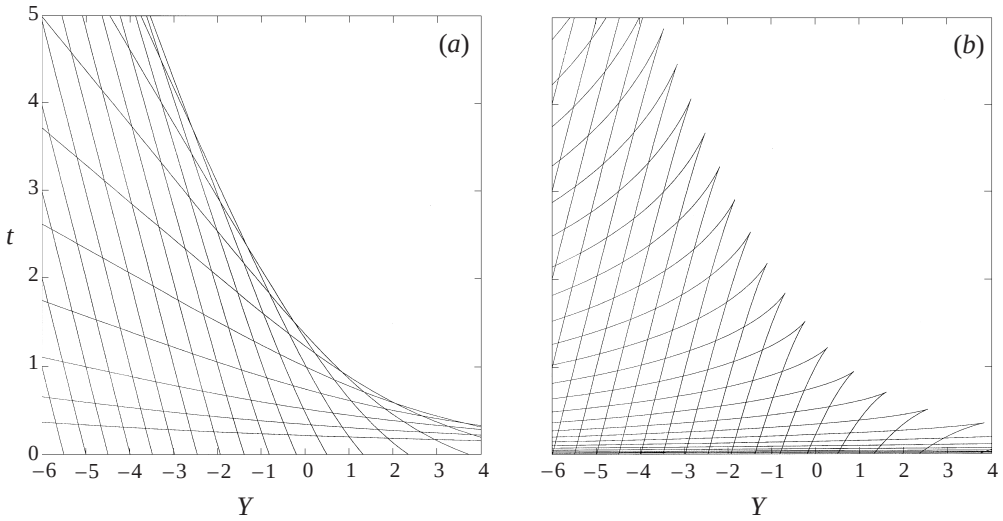


FIGURE 3. The characteristics for the MBO initial condition. (*a*) The $\alpha$-family. (*b*) The $\beta$-family.

Then

$$h_t = g_Y \ , \quad h^2 g_t = h_Y \ , \tag{4.6}$$

and the initial conditions become to leading order

$$\text{MBO:} \quad h = \frac{8}{(2+\mathrm{e}^{\eta})^2} \ , \quad g = 0 \ , \quad \text{where} \quad Y = \eta + \frac{\mathrm{e}^{\eta}}{2} \ ; \tag{4.7a}$$

$$\text{Krasny:} \quad h = 2 - 2\mathrm{e}^{Y} + \mathrm{e}^{2Y} \ , \quad g = -2\arctan\left(\frac{\mathrm{e}^{Y}}{2-\mathrm{e}^{Y}}\right) \ ; \tag{4.7b}$$

$$\text{Moore:} \quad h = 2 + \tfrac{1}{2}\mathrm{e}^{2Y} \ , \quad g = -2\arctan\left(\tfrac{1}{2}\mathrm{e}^{Y}\right) \ . \tag{4.7c}$$

As outlined in Appendix B, Professor D. W. Moore and Professor J. T. Stuart (private communication) have obtained an exact solution to (4.6) by means of a Hodograph transformation. We will employ their method to obtain the large time limit of the solution. However, in order to appreciate fully the motion of the singularities, it is also instructive to plot the characteristics of the hyperbolic system (4.6). This system has the Riemann invariants

$$a(\alpha) = h\mathrm{e}^{g} \quad \text{and} \quad b(\beta) = h\mathrm{e}^{-g} \ , \tag{4.8}$$

which are constants along the characteristics

$$\frac{\mathrm{d}Y}{\mathrm{d}t} = -\frac{1}{h} \quad \text{and} \quad \frac{\mathrm{d}Y}{\mathrm{d}t} = \frac{1}{h} \, , \tag{4.9}$$

respectively. The characteristic labels $\alpha$ and $\beta$ can be defined through the initial conditions. For instance, in the case of (4.7*c*) these can be fixed by requiring that $\alpha = \beta = \eta$ at $t = 0$; whence

$$a(\alpha) = \frac{8}{(2+\mathrm{e}^{\alpha})^2} \, , \quad b(\beta) = \frac{8}{(2+\mathrm{e}^{\beta})^2} \, . \tag{4.10}$$

Baker (1990) has previously obtained numerical solutions to (4.8)–(4.10). In figure 3 we illustrate both families of characteristics for the MBO initial condition. Not all the characteristics used for the calculation are displayed. The results show clearly the

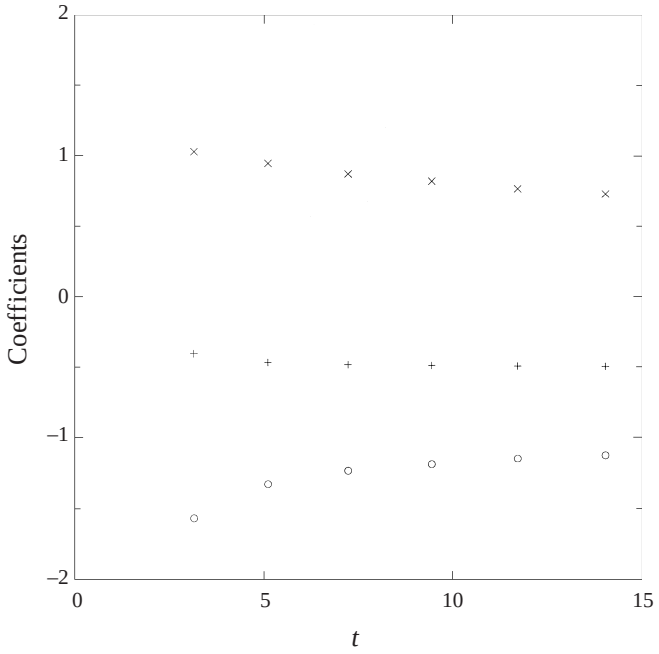


FIGURE 4. The coefficients of the form-fit to the envelope. +, $c_1$; ∘, $c_2$; ×, $c_3$.

formation of an envelope in the characteristics. The envelope marks out the trajectory of the singularity in $h$ and $g$ (and $s$), as it moves in from infinity. The small-time behaviour of this envelope is given by (2.20), while the large-time asymptotic position of the singularity, $Y_s$, is calculated in Appendix B. From (B 15), we see that

$$Y_s \sim -\tfrac{1}{2}t - \ln t + \ln 4 - 1\,, \tag{4.11}$$

while from (B 4), (B 16) and (B 17), we find that at the singularity

$$h = 2 - \frac{4}{t} + \dots\,, \quad g = -\frac{2}{t} + \dots\,. \tag{4.12}$$

Close to the singularity, it follows from (B 19) and (4.5), that the solution has the form

$$s_\xi \sim -\frac{(1-\mathrm{i})}{t}\left(1 - (2\mathrm{i}\xi - t - 2\ln(\epsilon t) + 4\ln 2 - 2)^{1/2} + \dots\right)\,. \tag{4.13}$$

In order to compare these asymptotic predictions with our numerical calculations, we determine the position of the envelope by seeking the nearest point along a $\beta$ characteristic where it changes direction abruptly (see figure 3*b*). We so obtain a sequence of points that lie closely on the envelope. Then we use the method of least squares to determine the coefficients in the form $Y = c_1 t + c_2 \ln t + c_3$. The fit is applied at a number of successive times, using 100 consecutive points to determine the best fit. These coefficients are plotted in figure 4 as a function of the midpoint of the time interval in which the local fit was made. We see that the coefficient $c_1$ quickly settles to $-\frac{1}{2}$ in agreement with the asymptotic result; similarly the coefficient $c_2$ appears to be approaching $-1$. However, while the coefficient $c_3$ is decreasing towards $(\ln 4 - 1)$, it is still much larger in value. This slow convergence is possibly not surprising given that $t$ must be very large in order for $\ln t$ to be large. We also check the behaviour of $h$ and $g$ along the envelope and find that $gt$ approaches $-2$

very quickly, but that $(2-h)t$ approaches 4 slowly. Nevertheless, it seems that the results are not inconsistent with the asymptotic predictions.

The asymptotic results (4.11) and (4.13) are for the MBO initial condition (4.7*a*). To the order given they are the same as those found by Moore (1979, 1985) for initial condition (4.7*c*). Further, using Moore's (1985) method, Krasny (1986*a*) found that for his initial condition, (4.7*b*), the only change in the expressions was in a constant, i.e. (4.11) became

$$Y_s \sim -\tfrac{1}{2}t - \ln t + \ln 2 - 1\,. \tag{4.14}$$

However, Moore's (1985) method of obtaining these expressions is based on finding an asymptotic solution to (4.3) using the small parameter $\epsilon$. Since we have seen that $\epsilon$ can be scaled from the problem within the assumptions of the asymptotic approximation, a (small) question mark hangs over Moore's (1985) analysis and the consequent results for initial conditions (4.7*b*) and (4.7*c*).

One way to confirm that these results are indeed correct, would be to find the required large-time asymptotic expressions from the exact solution in the Hodograph plane (cf. Appendix B). However, for initial conditions such as (4.7*b*) and (4.7*c*) for which $g \neq 0$ at $t = 0$, this is non-trivial. As an alternative approach, we have recast Moore's (1985) analysis in terms of a large-time asymptotic solution to (4.6) using the method of matched asymptotic expansions.† It turns out that the reason a self-consistent large-time asymptotic solution can be found, is that both the characteristics that intersect the singularity at large times intersect the $Y$-axis at asymptotically large values of $Y$ (at $Y = O(\ln t)$ and $Y = O(t)$ for the $\alpha$ and $\beta$ characteristics respectively). It is for the same reason that the expressions for $Y_s$ are so similar for the different initial conditions (4.7). While certain technical details of our solution differ from those of Moore (1985), e.g. the order at which particular terms appear in the expansion, the results (4.11), (4.13) and (4.14) stand.

As yet in this subsection, we have essentially only recovered Moore's (1979, 1985) results, albeit by more formal asymptotic means. However, as a result of our derivation it is clear that such results can only be valid while the singularity is far from the real $\xi$-axis. This is no longer true when $t$ is sufficiently large that

$$y_s \sim \ln(1/\epsilon) - \frac{t}{2} - \ln(t) = O(1)\,. \tag{4.15}$$

At this stage a new approach is necessary since the assumptions leading to (2.13) are not justifiable.

Before considering the solution at such times, in figure 5 we show the families of characteristics for the Krasny initial condition (4.7*b*). These were calculated using the same numerical method as Baker (1990), and again not all characteristics used for the calculation are displayed. Grid refinement suggests that the figure is graphically accurate. This time we see four envelopes of characteristics. The envelopes develop when singularities that were created at $t = 0+$, away from the imaginary axis, collide on the axis (see figure 2). As a result of the four-fold symmetry in the solutions for $A$ and $B$ given in § 2.4, more than one pair of singularities can collide. As illustrated in figure 5, the first collision results in two envelopes representing singularities that propagate in the direction of increasing $Y$. However, at a slightly later time, another collision results in singularities that propagate in the direction of decreasing $Y$ (i.e. in the direction of the real axis). As noted by Moore (1985) and Caflisch *et al.* (1993), once a collision has occurred the solution is multi-valued. The key part of the

† The analysis is available from the authors upon request.

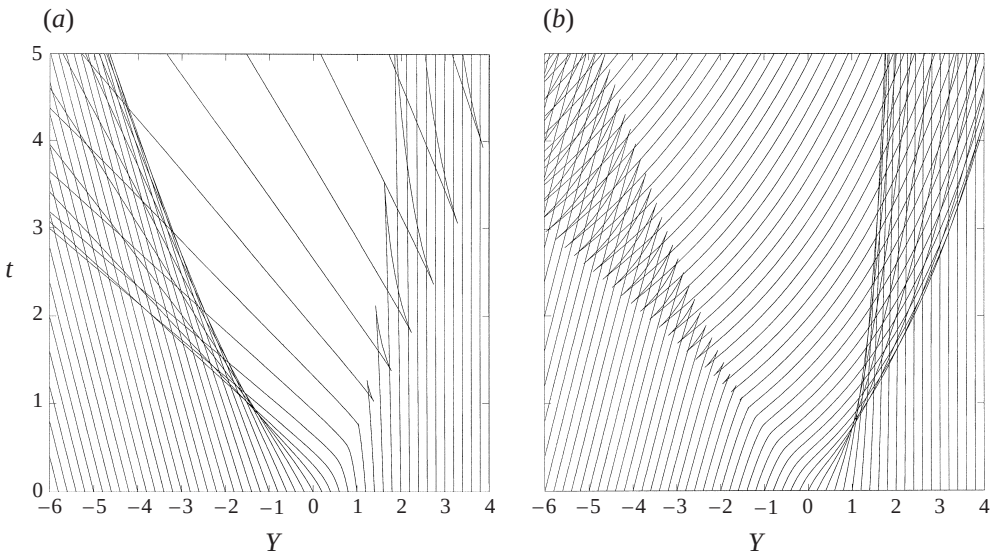


FIGURE 5. The characteristics for the Krasny initial condition. (*a*) The $\alpha$-family. (*b*) The $\beta$-family.

solution as far as we are concerned is that part that is on the same Riemann sheet as the physical solution at $Y = -\ln(1/\epsilon)$. This means that it is the slower of the two envelopes propagating in the direction of decreasing $Y$ that determines the behaviour on the real $\xi$-axis, i.e. it is the slower moving envelope that gives the trajectory of the 'closest' singularity to the real $\xi$-axis.

### 4.2. *The solution as the physical singularity forms*

As the singularity, and its complex conjugate, propagate towards the real $\xi$-axis, their 'amplitude' as given by (4.13) decreases. *Inter alia* this means that when the singularities are an order-one distance from the real $\xi$-axis, their effect on the interface is still small; indeed the numerical results of Krasny (1986*a*) and Shelley (1992) show that the interface is not significantly deformed. The combination of these facts suggests that the evolution of the vortex sheet at this stage should be governed by the linearized form of the Birkhoff–Rott equation (2.1).

The general solution of the linearized equation is well-known, so we just quote the relevant results. If we express the solution as a Fourier series

$$s(\xi, t) = \sum_{k=-\infty}^{\infty} \hat{s}_k(t) \exp(\mathrm{i}k\xi) \,, \tag{4.16}$$

then the Fourier coefficients are given by

$$\hat{s}_k(t) = (1+\mathrm{i})\hat{a}_k \exp\left(-\tfrac{1}{2}|k|(t-t_0)\right) + (1-\mathrm{i})\hat{b}_k \exp\left(\tfrac{1}{2}|k|(t-t_0)\right) \,, \tag{4.17}$$

where $\hat{a}_k$ and $\hat{b}_k$ are constants such that $\hat{a}_{-k} = \hat{a}_k^*$ and $\hat{b}_{-k} = \hat{b}_k^*$ (the superscript $^*$ here denotes a complex conjugate). An arbitrary shift in time, $t_0$, has been introduced as an aid to subsequent matching. Further, if we assume that the solution is antisymmetric about $\xi = 0$, i.e. that $s(-\xi, t) = -s(\xi, t)$ as in § 4.1, then $\hat{s}_{-k} = -\hat{s}_k$. This in turn implies that $\hat{a}_k^* = -\hat{a}_k$ and $\hat{b}_{-k} = \hat{b}_k^*$, i.e. that $\hat{a}_k$ and $\hat{b}_k$ are purely imaginary.

The solution to the linearized equations is known once $\hat{a}_k$ and $\hat{b}_k$ have been specified. For instance, if we were interested in the solution for times $t = O(1)$, then $\hat{a}_k$ and $\hat{b}_k$ can be determined from initial conditions such as (2.14) or (2.21); in the case of the MBO initial condition (with $t_0 = 0$), this leads to

$$\hat{a}_k = -\hat{b}_k = \frac{\epsilon}{4\pi \mathrm{i}} \int_{-\pi}^{\pi} \sin\xi(1 + \epsilon\cos\xi)\sin\left(k(\xi + \epsilon\sin\xi)\right)\,\mathrm{d}\xi\ . \tag{4.18}$$

While the solution given by (4.16) and (4.18) is valid for times $t = O(1)$, it is not uniformly valid for all time. As a result of cumulative nonlinear effects, the analysis in § 4.1 suggests that the 'constants' $\hat{a}_k$ and $\hat{b}_k$ have to be adjusted for times $t - t_\epsilon = O(1)$, where $t_\epsilon \gg 1$ is the solution of

$$t_\epsilon + 2\ln(t_\epsilon) = 2\ln(1/\epsilon)\ . \tag{4.19}$$

Hence, in order to describe the shape of the vortex sheet at the moment of singularity formation, our task is to identify the coefficients $\hat{a}_k$ and $\hat{b}_k$ when $t_0 = t_\epsilon$. In fact for our purposes it will be sufficient to find $\hat{a}_k$ and $\hat{b}_k$ for $|k| \gg 1$. Also, for definiteness we will fix on the MBO and Moore initial conditions, for both of which (4.11) and (4.13) are asymptotic approximations.

Since $t_\epsilon \gg 1$, we introduce a shifted time

$$t = t_\epsilon + \tau\ . \tag{4.20}$$

Then for large negative times $\tau$ such that $2\ln\epsilon \ll \tau \ll -1$, we know from matching to (4.13) that, in the neighbourhood of the singularity closest to the real $\xi$-axis, $s_\xi$ has the leading-order behaviour

$$s_\xi \sim \frac{\mathrm{i} - 1}{t_\epsilon}\left(1 - (2\mathrm{i}\xi - \tau + 4\ln 2 - 2)^{1/2} + \ldots\right)\ . \tag{4.21}$$

Further, in Appendix A we show that if the singularity of $s$ closest to the real $\xi$-axis has a branch-point singularity of the form (4.21), then the tail of the Fourier spectrum satisfies (see (A 5))

$$\hat{s}_k \sim \frac{1 + \mathrm{i}}{(2\pi)^{1/2} t_\epsilon} k^{-5/2} \exp\left(k\left(\tfrac{1}{2}\tau - \ln 4 + 1\right)\right) \quad \text{for} \quad k \gg 1\,. \tag{4.22}$$

The Fourier coefficients for $k$ large and negative follow from the antisymmetry condition $\hat{s}_{-k} = -\hat{s}_k$. The constants $\hat{a}_k$ and $\hat{b}_k$ for $|k| \gg 1$ can now be fixed, at least to leading order, by matching (4.22) with (4.17). In particular, we conclude that $\hat{a}_k = 0$ if the solution is not to grow exponentially as $\tau \to -\infty$, and that

$$\hat{b}_k = \frac{\mathrm{i}}{(2\pi)^{1/2} t_\epsilon} k^{-5/2} \exp\left(k\,(1 - \ln 4)\right) \quad \text{for} \quad k \gg 1\,. \tag{4.23}$$

Consequently it follows that for $|k| \gg 1$, the Fourier coefficients $\hat{s}_k$ are given by (4.22) for finite times $\tau = O(1)$, as well as for large negative times $2\ln\epsilon \ll \tau \ll -1$. Further, it is evident from (4.16) and (4.22) that the solution ceases to be analytic at $\tau = \tau_s \equiv 2(\ln 4 - 1)$.

Although we have not found the values of the $\hat{b}_k$ for $k = O(1)$, it is still possible to determine the shape of the vortex sheet in the neighbourhood of the singularity for

$(\tau_s - \tau) \ll 1$. In particular we note that

$$s_{\xi\xi\xi} = -2\mathrm{i}\sum_{k=1}^{\infty} k^2 \hat{s}_k \sin k\xi$$

$$\sim -2\mathrm{i}\sum_{k=1}^{\mathscr{K}} k^2 \hat{s}_k \sin k\xi + \frac{1-\mathrm{i}}{t_\epsilon} \sum_{k=\mathscr{K}+1}^{\infty} \left(\frac{2}{\pi k}\right)^{1/2} \exp\left(-\tfrac{1}{2}k\,(\tau_s - \tau)\right) \sin k\xi\,, \quad (4.24)$$

where $\mathscr{K}$ is a constant chosen such that $1 \ll \mathscr{K} \ll (\tau_s - \tau)^{-1}$. For $(\tau_s - \tau) \ll 1$, the dominant contribution to $s_{\xi\xi}$ comes from the second sum in (4.24). By approximating the sum by a Riemann integral (Bender & Orszag 1978), we thus find that in the vicinity of the curvature singularity

$$z_{\xi\xi\xi} = s_{\xi\xi\xi} \sim \frac{2(1-\mathrm{i})}{(\tau_s - \tau)^{1/2} t_\epsilon} \frac{\sin\left(\frac{1}{2}\arctan(2\chi)\right)}{(4\chi^2+1)^{1/4}} \quad (4.25)$$

$$\sim \frac{2\mathrm{e}^{-\mathrm{i}\pi/4}}{(\tau_s - \tau)^{1/2} t_\epsilon} \left(\frac{(4\chi^2+1)^{1/2} - 1}{4\chi^2 + 1}\right)^{1/2}, \quad (4.26)$$

where $\chi = \xi/(\tau_s - \tau)$ and $0 < (\tau_s - \tau) \ll 1$. It follows that at $\tau = \tau_s$

$$z_{\xi\xi\xi} \sim \frac{(1-\mathrm{i})\,\mathrm{sgn}\xi}{t_\epsilon |\xi|^{1/2}} \quad \text{for} \quad |\xi| \ll 1\,. \quad (4.27)$$

By focusing attention on each singularity individually, Moore (1979) has previously given an expression for $z$ valid in the neighbourhood of a (complex) singularity. However, his equation (5.5) includes an unknown function $\psi(\chi)$ that makes a significant contribution to $z$, and thence to $z_{\xi\xi\xi}$, when $\chi$ is real. By correctly including the effects of both singularities on either side of the real $\xi$-axis simultaneously, we have been able to calculate the leading-order contribution to this function $\psi$. Even so, the influence of the singularities on each other is not particularly strong; in particular they seem to have little influence on the speed that each moves at.† As a result Moore (1979) accurately predicted the time of singularity formation, $t_s = t_\epsilon + \tau_s$, without the need to consider both singularities simultaneously.

We test the asymptotic solutions by direct comparison with numerical simulations of (2.2) for the MBO initial condition with $\epsilon = 0.5$, 0.05, 0.005. We use the same numerical method as described in § 3. In each case, we use a filter level of $10^{-25}$, and start with $N = 32$ or $N = 64$ points. The filter level ensures that there is a wavenumber above which the amplitudes are set to zero. Whenever this wavenumber approaches $N/2$ we double the number of points; table 1 gives example ranges in time over which different spatial resolutions and time steps were used. Following Shelley (1992) we form fit

$$\frac{\mathrm{i}\mathscr{A}}{k^{5/2}} \exp(-\mathrm{Im}(\xi_s)k) \left(1 + \frac{\mathscr{B}}{k}\right) \quad (4.28)$$

to the spectrum of $x(\xi) - \xi$ and $y(\xi)$. This is the simplified form of (A 3) appropriate for the case where $\mu = 0$ and $\mathrm{Re}(\xi_s) = 0$, but with an additional factor to represent the next-order correction. For this part of the calculation we have also assumed that $\nu = 3/2$. These changes and refinements help in obtaining $\mathscr{A}$ and $\mathrm{Im}(\xi_s)$ more accurately. The symmetry in $x(\xi)$ and $y(\xi)$ results in both $\mathscr{A}$ and $\mathscr{B}$ being real.

† This is of course consistent with our linearization assumption.

| $\epsilon$ | $N$ | Range in time | Time step |
|---|---|---|---|
| 0.5 | 64 | $0 \leqslant t \leqslant 0.6$ | 0.0025 |
| | 128 | $0.6 \leqslant t \leqslant 1.1$ | 0.0025 |
| | 256 | $1.1 \leqslant t \leqslant 1.35$ | 0.0025 |
| | 512 | $1.35 \leqslant t$ | 0.0025 |
| 0.05 | 64 | $0 \leqslant t \leqslant 2.4$ | 0.0025 |
| | 128 | $2.4 \leqslant t \leqslant 3.3$ | 0.0025 |
| | 256 | $3.3 \leqslant t \leqslant 3.7$ | 0.0025 |
| | 512 | $3.7 \leqslant t$ | 0.0025 |
| 0.005 | 32 | $0 \leqslant t \leqslant 3.0$ | 0.01 |
| | 64 | $3.0 \leqslant t \leqslant 5.4$ | 0.01 |
| | 128 | $5.4 \leqslant t \leqslant 6.4$ | 0.005 |
| | 256 | $6.4 \leqslant t \leqslant 7.0$ | 0.005 |
| | 512 | $7.0 \leqslant t$ | 0.005 |

TABLE 1. Choice of numerical parameters.

In figure 6, we show $\mathrm{Im}(\xi_s)$, the location of the singularity on the imaginary axis, as a function of time for both the numerical solution to (2.2) and the asymptotic prediction (4.11):

$$\mathrm{Im}(\xi_s) = -\tfrac{1}{2}t - \ln(\epsilon t) + 2\ln(2) - 1\,. \tag{4.29}$$

As might be expected, the agreement between theory and numerical results improves as $\epsilon$ decreases. While the asymptotic prediction of the speed at which the singularity approaches the real axis is good, the prediction of the position tends to be too low. However it should be remembered that the asymptotic results depend on $(\ln(1/\epsilon))^{-1}$ being small, and $(\ln(1/\epsilon))^{-1} = 0.19$ for $\epsilon = 0.005$.

We delay a discussion of our numerical estimates of the coefficient $\mathscr{A}$ until after our discussion in § 5 of the form of the physical singularity for finite-amplitude disturbances.

## 5. The local form of the curvature singularity

The arguments leading up to (4.25) refer specifically to small-amplitude disturbances to a vortex sheet, such that the sheet remains flat to leading order up until the singularity forms. However, a generalization of (4.25) for the local structure of the singularity can be derived for larger deformations of the sheet.

As in § 4, identify the Lagrangian coordinate $\xi$ with the circulation (so that $\Gamma_\xi = 1$). Without loss of generality assume that the singularity forms at $t = 0$ and $\xi = 0$, and that the surface is moving with a velocity $\dot{z}_0$ at that point. We also assume that at the time of singularity formation, the surface is locally flat in the neighbourhood of the singularity, with $z \sim \lambda\xi$, where $\lambda$ is a complex number.

The asymptotic expansion of the solution to the Birkhoff–Rott equation (2.2) sought for $t \ll 1$ has two regions: a local region where $\xi = O(t)$, and an extensive region covering the rest of the sheet. In order to determine the local shape of the vortex sheet near the singularity, it is not necessary to consider the extensive region in detail, other than to note that in a Taylor expansion of $z(\xi, t)$ in powers of $t$, it is consistent to assume that the first two terms of the asymptotic expansion are $O(t^0)$ and $O(t^1)$ respectively; this assumption may be justified *a posteriori*.

As regards the local sheet shape in the region near the singularity, the key stage in

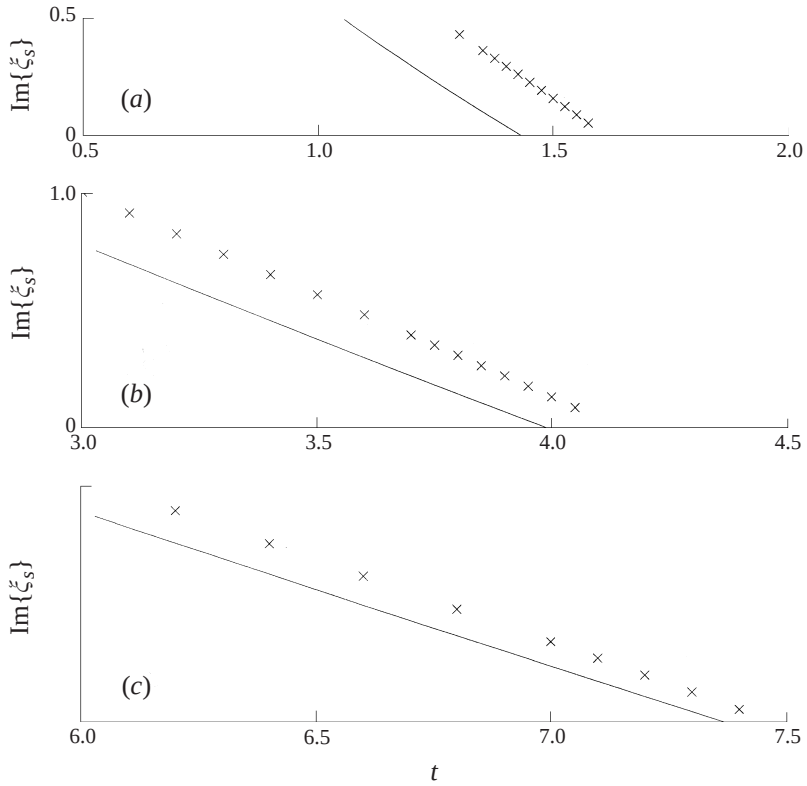


FIGURE 6. The location of the 'nearest' singularity on the imaginary axis for the MBO initial condition. We show three choices for $\epsilon$: (*a*) 0.5, (*b*) 0.05, (*c*) 0.005. ×, Numerical simulations; —, the asymptotic prediction (4.11).

the derivation of an asymptotic solution is the asymptotic evaluation for $|\xi| \ll 1$ of the Cauchy integral in (2.1). To this end, we split the integral into three parts:

$$\fint_{-\infty}^{\infty} \frac{\mathrm{d}\hat{\xi}}{z(\xi,t)-z(\hat{\xi},t)} = \left\{ \int_{-\infty}^{-\delta} + \fint_{-\delta}^{\delta} + \int_{\delta}^{\infty} \right\} \frac{\mathrm{d}\hat{\xi}}{z(\xi,t)-z(\hat{\xi},t)}, \tag{5.1}$$

where $|\xi| \ll \delta \ll 1$.

Initially we concentrate on the first and third integrals on the right of (5.1). As a result of the assumptions (*a*) that near the singularity the vortex sheet is approximately flat, and (*b*) that away from the singularity the first two terms of the asymptotic expansion for $z$ are $O(t^0)$and $O(t^1)$, it follows that the leading-order contribution from the first and third integrals is $O(t^0)$. Specifically for $|\xi| \ll \delta$ and $|t| \ll 1$,

$$\begin{aligned}
&\left\{ \int_{-\infty}^{-\delta} + \int_{\delta}^{\infty} \right\} \frac{\mathrm{d}\hat{\xi}}{z(\xi,t)-z(\hat{\xi},t)} \\
&\quad = \left\{ \int_{-\infty}^{-\delta} + \int_{\delta}^{\infty} \right\} \frac{1}{z(0,t)-z(\hat{\xi},t)} \left( 1 - \frac{z(\xi,t)-z(0,t)}{z(0,t)-z(\hat{\xi},t)} + \ldots \right) \mathrm{d}\hat{\xi} \\
&\quad = \left\{ \int_{-\infty}^{-\delta} + \int_{\delta}^{\infty} \right\} \frac{1}{z(0,0)-z(\hat{\xi},0)} \left( 1 - \frac{\lambda\xi}{z(0,0)-z(\hat{\xi},0)} + \ldots \right) \mathrm{d}\hat{\xi} \\
&\quad = \fint_{-\infty}^{\infty} \frac{\mathrm{d}\hat{\xi}}{z(0,0)-z(\hat{\xi},0)} - \fint_{-\delta}^{\delta} \frac{\mathrm{d}\hat{\xi}}{z(0,0)-z(\hat{\xi},0)} + O\left( |t|, \frac{|\xi|}{\delta} \right),
\end{aligned} \tag{5.2}$$

where the second integral is $O(\delta)$ or smaller as a result of the assumption that near the singularity the vortex sheet is approximately flat.

We now concentrate on the second integral on the right-hand side of (5.1), because it is this integral that determines the shape of the vortex sheet in the neighbourhood of the singularity. In order to obtain an asymptotic approximation of this integral, we first rescale it using

$$z = \dot{z}_0|\lambda|^2\tau + \lambda(\xi + s(\xi,\tau)) \,, \quad t = |\lambda|^2\tau \,, \tag{5.3}$$

where $s$ is slightly redefined from (2.4). The second integral then becomes

$$\begin{aligned} \fint_{-\delta}^{\delta} \frac{\mathrm{d}\hat{\xi}}{z(\xi,t) - z(\hat{\xi},t)} &= \frac{1}{\lambda} \fint_{-\delta-\xi}^{\delta-\xi} \frac{\mathrm{d}\zeta}{s(\xi,\tau) - s(\xi+\zeta,\tau) - \zeta} \\ &= \frac{1}{\lambda} \fint_{-\delta-\xi}^{\delta-\xi} \frac{s(\xi+\zeta,\tau) - s(\xi,\tau)}{\zeta + s(\xi+\zeta,\tau) - s(\xi,\tau)} \frac{\mathrm{d}\zeta}{\zeta} - \frac{1}{\lambda} \ln\left(\frac{\delta-\xi}{\delta+\xi}\right), \end{aligned} \tag{5.4}$$

where the final result follows from the identity

$$\fint_{-\delta-\xi}^{\delta-\xi} \frac{\mathrm{d}\zeta}{\zeta} = \ln\left(\frac{\delta-\xi}{\delta+\xi}\right). \tag{5.5}$$

On substitution of (5.3) into the Birkhoff–Rott equation (2.2), it follows from using (5.1), (5.2), (5.4) and the assumption that $\xi$ and $s$ are small, that to leading order in powers of $\tau$ and $\delta$,

$$\dot{z}_0 = \fint_{-\infty}^{\infty} \frac{\mathrm{d}\hat{\xi}}{z(0,0) - z(\hat{\xi},0)} \,; \tag{5.6}$$

i.e. the sum of the first and third integrals in (5.1) essentially balances the $\dot{z}_0$ term representing the velocity with which the singularity is moving.

At second order in powers of $\tau$, a scaling argument demonstrates that for a balance between the left- and right-hand sides to occur, the appropriate inner coordinate is (cf. (4.25))

$$\xi = (-\tau)\chi \,. \tag{5.7}$$

A similarity solution to the Birkhoff–Rott equation in the neighbourhood of the singularity is now sought of the form

$$s = (-\tau)^q F(\chi) + \dots \,, \tag{5.8}$$

where $q > 1$ in order to be consistent with the sheet being locally flat in the neighbourhood of the singularity. For simplicity we also assume that $q < 2$, because otherwise extra book-keeping terms need to be included in (5.2) and (5.8). We note that the curvature singularity discussed in the previous sections corresponds to $q = \frac{3}{2}$.

From use of (5.1)–(5.4) and (5.6)–(5.8), the asymptotic expansion of the Birkhoff–Rott equation (2.2) at $O(\tau^{q-1})$ yields

$$\chi\bar{F}_\chi - q\bar{F} = \frac{1}{2\pi\mathrm{i}} \int_{-\infty}^{\infty} \frac{F(\chi+\eta) - F(\chi)}{\eta^2} \,\mathrm{d}\eta \,. \tag{5.9}$$

We note that for the book-keeping that is required for asymptotic matching, the $O(\tau^{q-1})$ term is not necessarily the second term in the asymptotic expansion of this inner region. For instance, if $z$ is not antisymmetric about $\xi = 0$, then there will be a larger $O(\delta)$ term from, *inter alia*, the second integral in (5.2). However, because the final answer cannot depend on the artificial parameter $\delta$, we know that such

terms must cancel to zero (although the algebra needed to identify the cancellation may be non-trivial). In the special case when $z$ is antisymmetric about $\xi = 0$, the $O(\tau^{q-1})$ term *is* the second term in the asymptotic expansion if we choose $\delta$ such that $(-\tau)^{2-q} \ll \delta \ll 1$.

In order to match with the 'outer' region where $\xi = O(1)$, we anticipate that $F \sim F_{\pm}|\chi|^q$ as $\chi \to \pm\infty$, where $F_{\pm}$ are constants. Also, if the integral in (5.9) is to be well defined, we require that $F_- = -F_+$, i.e. that to leading order the function $F$ is antisymmetric as $|\chi| \to \infty$.

Equation (5.9) can be solved by splitting into real and imaginary parts. Writing $F = F_{\mathrm{r}} + \mathrm{i}F_{\mathrm{i}}$, we substitute into (5.9) and integrate by parts to obtain

$$\chi G'_+ - qG_+ = \frac{1}{2\pi} \int\!\!\!\!\!\!- _{-\infty}^{\infty} \frac{G'_+(\eta)}{\eta - \chi}\, \mathrm{d}\eta\,, \tag{5.10}$$

$$\chi G'_- - qG_- = -\frac{1}{2\pi} \int\!\!\!\!\!\!- _{-\infty}^{\infty} \frac{G'_-(\eta)}{\eta - \chi}\, \mathrm{d}\eta\,, \tag{5.11}$$

where

$$G_{\pm} = F_{\mathrm{r}} \pm F_{\mathrm{i}}\,. \tag{5.12}$$

Let the Fourier transform of $G_{\pm}$ be defined by

$$\hat{G}_{\pm}(k) = \int_{-\infty}^{\infty} G_{\pm}(\chi) \exp(-\mathrm{i}k\chi)\, \mathrm{d}\chi\,. \tag{5.13}$$

Relatively straightforward algebraic manipulation of (5.10) and (5.11) using generalized functions leads to the conclusion that for $k > 0$

$$\hat{G}_{\pm} = \mathscr{G}_{\pm} k^{-q-1} \exp\left(\pm k/2\right)\,, \tag{5.14}$$

where the $\mathscr{G}_{\pm}$ are arbitrary complex constants. Since the $G_{\pm}(\chi)$ are real, the solution for $k < 0$ is given by $\hat{G}_{\pm}(k) = \hat{G}^*_{\pm}(-k)$, where the superscript $^*$ here denotes a complex conjugate.

In order that the Fourier transforms be invertible, we conclude that $\mathscr{G}_+ = G_+ = 0$. Performing the inversion for $\hat{G}_-$, and imposing the condition that at leading order $F$ is antisymmetric as $|\chi| \to \infty$, we conclude from (5.12), (5.13) and (5.14) that in the neighbourhood of the singularity, the departure of shape of the interface from a straight line is given by

$$F = \gamma(1 - \mathrm{i})(4\chi^2 + 1)^{q/2} \sin(q \arctan(2\chi))\,, \tag{5.15}$$

where $\gamma = -\mathrm{i}2^{-q}\Gamma(-q)\mathscr{G}_-$ is a real constant ($\mathscr{G}_-$ is purely imaginary).

Hence a self-consistent interface shape has been found for $1 < q < 2$. Further it appears that the value of $q$ is not fixed by higher-order terms. Indeed, depending on the initial condition, singularities of varying forms can develop on the interface (Duchon & Robert 1988; Caflisch & Orellana 1989; Caflisch & Semmes 1990). However, for the class of initial conditions studied in § 2, we would anticipate that $q = 3/2$, in which case it follows from (5.3), (5.7), (5.8) and (5.15) that (cf. (4.25))

$$z_\xi \sim \lambda + 3\gamma(1 - \mathrm{i})\lambda(-\tau)^{1/2}(4\chi^2 + 1)^{1/4} \cos\left(\tfrac{1}{2} \arctan(2\chi)\right)\,, \tag{5.16a}$$

$$z_{\xi\xi} = \lambda s_{\xi\xi} \sim 3\sqrt{2}\gamma\lambda \exp(-\mathrm{i}\pi/4)(-\tau)^{-1/2}(4\chi^2 + 1)^{-1/4} \sin\left(\tfrac{1}{2} \arctan(2\chi)\right)\,. \tag{5.16b}$$

These expressions possibly provide an explanation of Shelley's (1992) observation

| $\epsilon$ | $t_s$ | $\lambda$ | $\gamma$ |
|---|---|---|---|
| 0.5 | 1.614 | 0.4491 exp(i0.7990) | 0.1930−i 0.0033 |
| 0.2 | 2.495 | 0.5576 exp(i0.6364) | 0.2044−i 0.0076 |
| 0.05 | 4.145 | 0.6749 exp(i0.4338) | 0.1760−i 0.0055 |
| 0.005 | 7.476 | 0.7623 exp(i0.0261) | 0.1246−i 0.0242 |

TABLE 2. The singularity time, vortex-sheet slope and numerical strength of the curvature singularity for different disturbance amplitudes.

that when $\epsilon = 0.5$ in the MBO initial condition (2.14), the nature of the singularity in the real variable $y = \mathrm{Im}(z)$ seems to be different from that in the real variable $x = \mathrm{Re}(z)$. To this end we note from (5.16) that if the vortex sheet is inclined at 45° to the horizontal at the point where the singularity forms, i.e. if $\arg(\lambda) = \pi/4$, then the leading-order branch-cut singularity will only be evident in $x$, and not in $y$. Hence an explanation of Shelley's (1992) observation follows if the vortex sheet is inclined at approximately 45° when the singularity forms for $\epsilon = 0.5$.

In order to confirm this prediction we have repeated Shelley's (1992) numerical calculations for the MBO initial condition (2.14). We estimate the singularity time $t_s$ by using a least-squares form-fit,

$$t = t_s + a\mathrm{Im}(\xi_s) + b\mathrm{Im}(\xi_s)^2 + c\mathrm{Im}(\xi_s)^3\,, \tag{5.17}$$

to the numerical results shown in figure 6. We vary both the number of data points (typically seven), and the number of terms in the form-fit, in order to assess the sensitivity of the results. Once $t_s$ is known, we perform a least-squares form-fit of our numerical results for $z_\xi(0,t)$ to the asymptotic prediction from (5.16*a*):

$$z_\xi(0,t) = \lambda + 3\gamma(1-\mathrm{i})\frac{\lambda}{|\lambda|}(t_s - t)^{1/2} + \ldots\,. \tag{5.18}$$

In particular values of the derivative for typically seven times close to singularity formation are form-fitted to a complex-coefficient, fourth-order polynomial in powers of $(t_s - t)^{1/2}$. In table 2, we give results for $t_s$, $\lambda$ and $\gamma$ for several choices of $\epsilon$.

The accuracy of these results is difficult to assess because there are several places where errors can occur. This is especially so given that the singularity time $t_s$ is determined by a form-fit to results that are obtained by a form-fit to a numerical solution, and that $\lambda$ and $\gamma$ are then found from a form-fit involving $t_s$. Our checks show that changes in the resolution used in the calculation of the vortex sheet produce variations mostly in the third digit, as do variations in the number of terms and points used in the form-fits (the form-fit for $t_s$ being the most reliable). The exception is the case $\epsilon = 0.005$, where the length of the time integration gives data that lead to uncertainty in the second digit.

A key test of the asymptotic theory, and our explanation of Shelley's (1992) observation, is that $\gamma$ should be real; the results for $\mathrm{Im}(\gamma)$ in table 2 confirm that this is the case within the uncertainties in the numerical results. Moreover for $\epsilon = 0.5$ we note that the vortex sheet is inclined at approximately 45° when the singularity forms. Thus, our numerical results are consistent both with the asymptotic theory, and with our explanation of why the singularity in $y$ appears to be different from that in $x$ when $\epsilon = 0.5$.

## 6. Conclusions

One of the motivations for this paper was a desire to understand the asymptotic shape of the vortex sheet just prior to the formation of Moore's curvature singularity. In due course we hope that an accurate knowledge of this shape will aid in the understanding of the motion of the vortex sheet in the case of regularized, or well-posed, modifications of the problem.

In pursuing our aim we have obtained an asymptotic solution for the evolution of small sinusoidal disturbances to a vortex sheet up to the time at which the curvature singularity develops. *Inter alia*, this has enabled us to obtain the shape of the vortex sheet as the singularity develops. In particular we have identified the function $\psi$ left unspecifed in equation (5.5) of Moore's (1979) paper.

Without necessarily assuming that the vortex sheet is only slightly deformed, we have also found a local asymptotic description of a family of curvature singularities. A feature of this family of singularities is that the interface shape is governed by a *linear* equation, i.e. (5.9). The local analysis in § 5 does not uniquely specify the strength of the singularity – a property that depends, *inter alia*, on the initial conditions. For instance, if at $t = 0$ a singularity with $q > 1$ exists in the complex $\xi$-plane, the singularity can in principle propagate towards, and then intersect, the real $\xi$-axis without changing its strength (Duchon & Robert 1988; Caflisch & Orellana 1989; Caflisch & Semmes 1990). However, we have also shown in § 2, that even if there are no complex singularities in the initial condition at $t = 0$, singularities with $q = 3/2$ can spontaneously develop at $t = 0+$. As for the local singularity analysis in § 5, this result does not depend on the initial disturbance to the vortex sheet being small. Further, we believe that this spontaneous development of $\frac{3}{2}$-power singularities at $t = 0+$ means that such singularities are possibly the most likely to be seen in practice. However, as a note of caution we recall that our analysis is based on the assumption that the integrals (2.7*b*) and (2.8*b*) do not contribute to the singularity structure. As indicated in § 2.1 this might not always be the case if the integration contour cannot be suitably deformed.

Finally we note a paradox. Viewed as a problem on the real $\xi$-axis, the evolution of small sinusoidal disturbances of amplitude $\epsilon$ to a vortex sheet is initially a linear problem. Then over a time $t = O(\ln(1/\epsilon))$ the cumulative effect of nonlinearity is to generate a Moore curvature singularity. However, viewed in appropriate parts of the complex plane, the problem is nonlinear for $t = O(1)$ (including of course the crucial spontaneous formation of singularities at $t = 0+$) and linear thereafter!

The authors are especially grateful to Professor D. W. Moore and Professor J. T. Stuart both for their interest, and for their help with Appendix B. The authors also wish to acknowledge valuable discussions with Professor R. E. Caflisch, Professor P. G. Saffman, Dr M. Siegel and other attendees of the informal workshop held on the occasion of Professor D. W. Moore's 59th birthday (Caltech, 1990). S.J.C. thanks Dr M. A. Page for helpful comments and financial support during visits to Monash University in 1989 and 1991, Professor P. G. Saffman and Caltech for financial support in 1990, and the Royal Society for an equipment grant. S.T. received support from the National Science Foundation (DMS-9500986) and also the Isaac Newton Institute, where he was a visitor in April–June 1995. Some of the calculations were performed at the Ohio Supercomputer Center, whose grant of computing resources is gratefully acknowledged. This work was presented at the NATO ARW on 'Singularities in Fluids, Plasmas and Optics' (Heraklion, 1992).

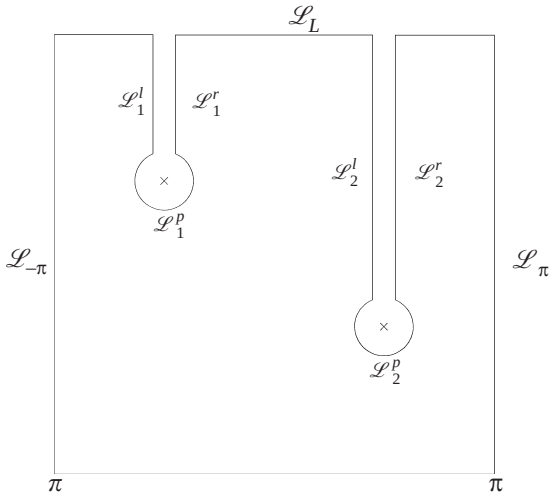


FIGURE 7. The integration contour for (A 1).

## Appendix A. The tail of the Fourier spectra

As shown in Carrier *et al.* (1966), the presence of singularities in the complex plane determine the dominant behaviour of the Fourier coefficients for large $|k|$. We briefly review their analysis by considering the integral

$$\hat{H}_k = \frac{1}{2\pi}\int_{-\pi}^{\pi} H(\xi)\mathrm{e}^{-\mathrm{i}k\xi}\,\mathrm{d}\xi = \frac{1}{2\pi}\int_{\mathscr{L}} H(\xi)\mathrm{e}^{-\mathrm{i}k\xi}\,\mathrm{d}\xi\,, \tag{A 1}$$

for which singularities of $H$ in the upper/lower half-plane determine the tail of the Fourier spectrum for negative/positive values of $k$ respectively. We consider the contour $\mathscr{L}$ illustrated in figure 7 and focus on large negative values of $k$. Branch-point singularities are assumed to be present at the locations marked with '$\times$'. The contour goes around these singularities as shown, and along either side of their branch cuts. Only two such singularities are illustrated, but there could be any finite number of them without affecting the following results. We assume that in the neighbourhood of the singularity closest to the real axis

$$H \sim \mathscr{H}(\xi)(\xi-\xi_s)^{\nu+\mathrm{i}\mu} + \mathscr{I}(\xi)\,, \tag{A 2}$$

where $\mathscr{H}(\xi)$ and $\mathscr{I}(\xi)$ are analytic at $\xi=\xi_s$. No singularity other than those marked in figure 7 is assumed to be present.

The two choices for $H(\xi)$ that we consider are $s(\xi,t)$ and $s_{\xi}(\xi,t)$ for some fixed $t$. In either case, $H(\xi)$ is $2\pi$-periodic, so the contributions from $\mathscr{L}_{-\pi}$ and $\mathscr{L}_{\pi}$ cancel. On the assumption that the branch-point singularities have powers greater than $-1$, the contributions from the integrals $\mathscr{L}_1^p$ and $\mathscr{L}_2^p$ also vanish as these contours shrink to zero radius.

Further, for $k<0$ and $|k|\gg 1$ the leading-order contribution to the integral comes from the asymptotically small section of these remaining contours closest to the real $\xi$-axis. In particular, if the singularity closest to the origin at $\xi=\xi_s$ is enclosed by $\mathscr{L}_2^p$, it follows from considering the lower ends of the contours $\mathscr{L}_2^r$ and $\mathscr{L}_2^l$ that

$$\hat{H}_k \sim -\frac{\mathscr{H}(\xi_s)\mathrm{e}^{-\mathrm{i}k\xi_s-\mathrm{i}(\nu+\mathrm{i}\mu)\pi/2}}{\pi(-k)^{1+\nu+\mathrm{i}\mu}}\sin((\nu+\mathrm{i}\mu)\pi)\Gamma(\nu+\mathrm{i}\mu+1)\,, \tag{A 3}$$

where $\Gamma$ is the Gamma function (rather than the circulation). Because the rate of decay in the exponential is determined by the distance of the singularity from the real $\xi$-axis, the contribution from the singularity closest to the real $\xi$-axis dominates contributions from other singularities. Similarly contributions from $\mathscr{L}_L$ are also asymptotically smaller than (A 3) as long as $(L - \mathrm{Im}(\xi_s)) \gg |k|^{-1}$.†

There are two different circumstances where we will use (A 3). The first occurs when the singularity lies on the imaginary axis and $\mu = 0$. In particular, the singularity in (4.21) has the form of (A 2) with $\mathscr{H}(\xi_s) = 2/t_\epsilon$, $\xi_s = (-\tau/2 + \ln 4 - 1)\mathrm{i}$ and $\nu = 1/2$. Hence the tail of the Fourier spectrum has the asymptotic behaviour

$$\mathrm{i}k\hat{s}_k \sim -\frac{(1-\mathrm{i})\exp(-k(\frac{1}{2}\tau - \ln 4 + 1)}{(2\pi)^{1/2} t_\epsilon (-k)^{3/2}} \quad \text{for} \quad k < 0,\ |k| \gg 1\,. \tag{A 4}$$

From the antisymmetry condition $\hat{s}_k = -\hat{s}_{-k}$ it follows that

$$\hat{s}_k \sim \frac{(1+\mathrm{i})\exp\left(k\left(\frac{1}{2}\tau - \ln 4 + 1\right)\right)}{(2\pi)^{1/2} t_\epsilon k^{5/2}} \quad \text{for} \quad k \gg 1\,. \tag{A 5}$$

The other time we use (A 3) is when singularities occur at $\xi_s$ and $-\bar{\xi}_s$. From the symmetry properties, and the definition of $s^*$, we have that $s^*(-\bar{\xi}_s) = \overline{s(-\xi_s)} = -\overline{s(\xi_s)}$. Hence if $s$ and $s^*$ have singularities of power $(\nu + \mathrm{i}\mu)$ at $\xi_s$, they have singularities of power $(\nu - \mathrm{i}\mu)$ at $-\bar{\xi}_s$. Further, the Fourier coefficients take their simplest form if we consider quantities that are real on the real $\xi$-axis, e.g. $H = \frac{1}{2}(s + s^*)$; the antisymmetry then implies that $\mathscr{H}(-\bar{\xi}_s) = -\overline{\mathscr{H}(\xi_s)}\exp(\mathrm{i}(\nu - \mathrm{i}\mu)\pi)$. By adding two contributions of the form (A 3), we find that for $k < 0$, $|k| \gg 1$, the tail of the spectrum has the asymptotic form

$$\hat{H}_k \sim \frac{2\mathrm{i}\mathscr{P}}{\pi(-k)^{1+\nu}} \exp(\mathrm{Im}(\xi_s)k)\sin(\mathrm{Re}(\xi_s)k + \mu\ln(-k) + \phi)\,, \tag{A 6}$$

where the real constants $\mathscr{P}$ and $\phi$ are given by

$$\mathscr{P}\mathrm{e}^{-\mathrm{i}\phi} = \mathscr{H}(\xi_s)\mathrm{e}^{-\mathrm{i}(\nu+\mathrm{i}\mu)\pi/2}\sin((\nu + \mathrm{i}\mu)\pi)\Gamma(\nu + \mathrm{i}\mu + 1)\,. \tag{A 7}$$

The form of the tail for $k \gg 1$ follows from the antisymmetry condition $\hat{H}_{-k} = -\hat{H}_k$.

## Appendix B. The long-time behaviour of the envelope

Professor D. W. Moore and Professor J. T. Stuart (private communication) use the Hodograph transformation to solve (4.6) for Moore's initial condition. We follow their approach for the MBO initial condition.

By interchanging the independent and dependent variables, the governing equations in the Hodograph plane are found to be

$$\frac{\partial t}{\partial h} = \frac{\partial Y}{\partial g} \quad \text{and} \quad \frac{\partial Y}{\partial h} = \frac{1}{h^2}\frac{\partial t}{\partial g}\,, \tag{B 1}$$

subject to the 'initial' conditions on $g = 0$

$$t(0,h) = 0 \quad \text{and} \quad Y(0,h) = \eta + \tfrac{1}{2}\mathrm{e}^{\eta}\,, \tag{B 2}$$

† The asymptotic behaviour of $s(\xi,t)$ for arbitrary large $\mathrm{Im}(\xi)$ is sometimes hard to identify. This is because the spontaneous generation of singularities at $t = 0+$ might lead to instantaneous significant departures from the initial condition at large values of $\mathrm{Im}(\xi)$ (e.g. Kunka, Foster & Tanveer 1997). Without loss of generality we therefore also assume that $(L - \mathrm{Im}(\xi_s)) = O(1)$.

where

$$e^{\eta} = 2((2/h)^{1/2} - 1) \quad \text{for} \quad 0 \leqslant h \leqslant 2\,. \tag{B 3}$$

We introduce new variables

$$h = 2e^{-2\rho}\,, \quad g = -2v\,, \quad t = e^{-\rho}\hat{t}(\rho, v)\,, \tag{B 4}$$

and eliminate $Y$ to obtain the Klein–Gordon equation

$$\frac{\partial^2 \hat{t}}{\partial \rho^2} - \frac{\partial^2 \hat{t}}{\partial v^2} - \hat{t} = 0\,. \tag{B 5}$$

From (B 1)–(B 3) the initial conditions become

$$\hat{t}(0, \rho) = 0\,, \quad \frac{\partial \hat{t}}{\partial v}(0, \rho) = \frac{1}{1 - \exp(-\rho)} \quad \text{for} \quad 0 \leqslant \rho < \infty\,. \tag{B 6}$$

By using Riemann's method of characteristics (e.g. Ince 1987), the solution may be expressed as

$$\hat{t}(\rho, v) = \int_{\rho - v}^{\rho + v} \frac{J_0\,(r(s; \rho, v))}{1 - \exp(-s)}\,\mathrm{d}s\,, \quad \text{where} \quad r(s; \rho, v) = (v^2 - (s - \rho)^2)^{1/2}\,, \tag{B 7}$$

where $J_0$ is the Bessel function of zero order. We are interested in the solution for $\hat{t} > 0$. To this end we note from (B 6) that $\partial \hat{t}/\partial v > 0$ on $v = 0$. This suggests that we should examine the solution in the region of coordinate space $0 \leqslant v \leqslant \rho$.

Our aim is an analytical expression for large times of the nature of the envelope in figure 3. Since $\hat{t}$ is large when $\rho - v \ll 1$, it is helpful to change the integration variable in (B 7) to $p = s - \rho + v$, to obtain

$$\hat{t} = \int_0^{2v} \frac{J_0\,(\hat{r}(p; v))}{1 - \exp(v - \rho - p)}\,\mathrm{d}p\,, \tag{B 8}$$

where $\hat{r}^2(p; v) = 2vp - p^2$. We will also need an expression for $Y$; from (B 1) and (B 4) we obtain

$$\frac{\partial Y}{\partial v} = \tfrac{1}{2}e^{\rho}\left(\frac{\partial \hat{t}}{\partial \rho} - \hat{t}\right)\,, \tag{B 9}$$

and hence

$$Y = \eta + \tfrac{1}{2}e^{\eta} - \tfrac{1}{2}e^{\rho}\int_0^v \mathrm{d}q \int_0^{2q} \mathrm{d}p\, \frac{J_0\,(\hat{r}(p; v))}{(1 - \exp(v - \rho - p))^2}\,, \tag{B 10}$$

where $e^{\eta} = 2(e^{\rho} - 1)$.

The numerical results in § 4 indicate that $h = 2e^{-2\rho} \approx 2$ on the envelope at large times. Hence we now asymptotically expand (B 8) and (B 10) on the assumption that $0 \leqslant v \leqslant \rho \ll 1$, to obtain

$$\hat{t} \sim \ln(\rho + v) - \ln(\rho - v) + v\,, \tag{B 11}$$

and

$$Y \sim \tfrac{1}{2}(\ln(\rho + v) + \ln(\rho - v)) + \ln 2 - \tfrac{1}{2}v(\ln(\rho + v) - \ln(\rho - v))\,. \tag{B 12}$$

Using (B 4), we find that

$$Y \sim -\tfrac{1}{2}t + \ln(\rho + v) + \ln 2 - \tfrac{1}{2}(\rho + v)t\,. \tag{B 13}$$

The envelope occurs where the determinant of the Jacobian of the mapping vanishes,

i.e. where

$$\frac{\partial t}{\partial h}\frac{\partial Y}{\partial g} = \frac{\partial t}{\partial g}\frac{\partial Y}{\partial h}\,.$$

Using (B 1) to eliminate the derivatives of $Y$, we can write this result in terms of the new variables as

$$\frac{\partial \hat{t}}{\partial v} = \pm\left(\frac{\partial \hat{t}}{\partial \rho} - \hat{t}\right).$$

From (B 11) this condition can in turn be written at large times as

$$\frac{2\rho}{\rho^2 - v^2} + 1 \sim \pm\left(-\frac{2v}{\rho^2 - v^2} - \ln(\rho + v) + \ln(\rho - v)\right).$$

If this expression is to have a solution with $0 \leqslant v \leqslant \rho$, then the lower sign must be taken. Further, we conclude from (B 4) and (B 11), that on the envelope

$$(\rho - v) \ll \rho\,, \quad \text{and} \quad \frac{2}{\rho + v} \sim (1 + \rho)t + 1\,. \tag{B 14}$$

On substituting (B 11) and (B 14) into (B 12), we find that the position of the singularity, $Y_s$, is given by

$$Y_s \sim -\tfrac{1}{2}t - \ln t + \ln 4 - 1\,. \tag{B 15}$$

In order to determine the nature of the singularity, we first note from (B 14) that $\rho \sim 1/t$ at the singularity. We therefore introduce a scaled variable $\hat{\rho}$ measured from the singularity

$$\rho = \frac{(1 - \hat{\rho})}{t}\,, \quad \text{where} \quad 0 < \hat{\rho} \ll 1\,. \tag{B 16}$$

From (B 4) and (B 11) it follows that

$$\rho - v = O(\exp(-t)/t)\,, \tag{B 17}$$

and hence from (B 13), (B 15) and (B 16) that

$$Y \sim Y_s - \tfrac{1}{2}\hat{\rho}^2\,. \tag{B 18}$$

We thus conclude from (4.2), (B 4), and (B 16)–(B 18) that close to the singularity

$$s_\xi = -1 + \exp(-\rho + \mathrm{i}v) \sim -\rho + \mathrm{i}v \sim \frac{(\mathrm{i} - 1)}{t}\left(1 - (2(Y_s - Y))^{1/2}\right), \tag{B 19}$$

where the choice of branch of the square-root ensures that the solution is on the same Riemann sheet as the physical domain (corresponding to $Y \to -\infty$).

## REFERENCES


Baker, G. R. 1983 Generalized vortex methods for free-surface flows. In *Waves on Fluid Interfaces* (ed. R. E. Meyer). Academic.

Baker, G. R. 1990 Singularities in the complex physical plane. In *Hyperbolic Problems* (ed. B. Engquist & B. Gustafson). Lund: Studentlitteratur.

Baker, G. R., Caflisch, R. E. & Siegel, M. 1993 Singularity formation during Rayleigh–Taylor instability. *J. Fluid Mech.* **252**, 51–78.

Baker, G. R. & Nachbin, A. 1998 Stable numerical methods for vortex-sheet motion in the presence of surface tension. *SIAM J. Sci. Comput.* (to appear).

Baker, G. R. & Shelley, M. J. 1990 On the connection between thin vortex layers and vortex sheets. *J. Fluid Mech.* **215**, 161–194.

Bender, C. M. & Orszag S. A. 1978 *Advanced Mathematical Methods for Scientists and Engineers.* McGraw-Hill.

Birkhoff, G. 1962 Helmholtz and Taylor instability. *Proc. Symp. Appl. Math. Am. Maths Soc.* **13**, 55–76.

Caflisch, R. E., Ercolani, N., Hou, T. Y. & Landis, Y. 1993 Multi-valued solutions and branch point singularities for nonlinear hyperbolic or elliptic systems. *Commun. Pure Appl. Maths* **46**, 453–499.

Caflisch, R. E. & Lowengrub, J. S. 1989 Convergence of the vortex method for vortex sheets. *SIAM J. Numer. Anal.* **26** 1060–1080.

Caflisch, R. E. & Orellana, O. F. 1986 Long time existence for a slightly perturbed vortex sheet. *Commun. Pure Appl. Maths* **39**, 1–18.

Caflisch, R. E. & Orellana, O. F. 1989 Singular solutions and ill-posedness for the evolution of vortex sheets. *SIAM J. Math. Anal.* **20**, 293–307.

Caflisch, R. E., Orellana, O. F. & Siegel, M. 1990 A localized approximation method for vortical flows. *SIAM J. Appl. Maths* **50**, 1517–1532.

Caflisch, R. E. & Semmes, S. 1990 A nonlinear approximation for vortex sheet evolution and singularity formation. *Physica* D **41**, 197–207.

Carrier, G. F., Krook, M. & Pearson, C. E. 1966 *Functions of a Complex Variable*. McGraw-Hill.

Delort, J.-M. 1991 Existence de nappes de tourbillon en dimension deux. *J. Am. Math. Soc.* **4**, 553–586.

Duchon, J. & Robert, O. 1988 Global vortex-sheet solutions of Euler equations in the plane. *J. Diffl Equat.* **73**, 215–224.

Ebin, D. G. 1987 The equations of motion of a perfect fluid with free-boundary are not well posed. *Commun. Part. Diffl Equat.* **12**, 1175–1201.

Ebin, D. G. 1988 Ill-posedness of the Rayleigh–Taylor and Helmholtz problems for incompressible fluids. *Commun. Part. Diffl Equat.* **13**, 1265–1295.

Hou, T. Y., Lowengrub, J. S. & Shelley, M. J. 1997 The long-time motion of vortex sheets with surface tension. *Phys. Fluids* **9**, 1933–1954.

Ince, E. L. 1987 *The Solution of Ordinary Differential Equations.* Longman Scientific & Technical.

Ishihara, T. & Kaneda, Y. 1994 Spontaneous singularity formation in the shape of vortex sheet in three-dimensional flow. *J. Phys. Soc. Japan* **63**, 388–392.

Ishihara, T. & Kaneda, Y. 1995 Singularity formation in three-dimensional motion of a vortex sheet. *J. Fluid Mech.* **300**, 339–366.

Krasny, R. 1986*a* A study of singularity formation in a vortex sheet by the point vortex method. *J. Fluid Mech.* **167**, 65–93.

Krasny, R. 1986*b* Desingularisation of periodic vortex-sheet roll-up. *J. Comput. Phys.* **65**, 292–313.

Kunka, M. D., Foster, M. R. & Tanveer, S. 1997 Dendritic crystal growth for weak undercooling. *Phys. Rev.* E **56**, 3068–3100.

Liu, J.-G. & Xin, Z. 1995 Convergence of vortex methods for weak solutions to the 2D Euler equations with vortex sheet data. *Commun. Pure Appl. Maths* **48**, 611–628.

Lundgren, T. S. 1982 Strained spiral vortex model for turbulent fine structure. *Phys Fluids* **25**, 2193.

Majda, A. 1993 Remarks on weak solutions for vortex sheets with a distinguished sign. *Indiana Univ. Math. J.* **42**, 921–939.

Meiron, D. I., Baker, G. R. & Orszag, S. A. 1982 Analytic structure of vortex-sheet dynamics. Part 1. Kelvin–Helmholtz instability. *J. Fluid Mech.* **114**, 283–298 (referred to herein as MBO).

Moore, D. W. 1978 The equation of motion of a vortex layer of small thickness. *Stud. Appl. Maths* **58**, 119–140.

Moore, D. W. 1979 The spontaneous appearance of a singularity in the shape of an evolving vortex sheet. *Proc. R. Soc. Lond.* A **365**, 105–119.

Moore, D. W. 1985 Numerical and analytical aspects of Helmholtz instability. In *Theoretical and Applied Mechanics, Proc. XVI ICTAM* (ed. F. I. Niordson & N. Olhoff). North-Holland.

Nie, Q. & Baker, G. R. 1998 Application of adaptive quadrature to axi-symmetric vortex-sheet motion. *J. Comput. Phys.* (to appear).

Nishida, T. 1977 A note on a theorem of Nirenberg. *J. Diffl Geom.* **12**, 629–633.

NITSCHE, M. 1998 Axisymmetric vortex sheet motion: Accurate evaluation of the principal value integral. Submitted.

PUGH, D. A. 1989 Development of vortex sheets in Boussinesq flows – formation of singularities. PhD Thesis, University of London.

PULLIN, D. I. 1982 Numerical studies of surface-tension effects in non-linear Kelvin–Helmholtz and Rayleigh–Taylor instability. *J. Fluid Mech.* **119**, 507–532.

SAFFMAN, P. G. & BAKER, G. R. 1979 Vortex Interactions. *Ann. Rev. Fluid Mech.* **11**, 95–122.

SHELLEY, M. J. 1992 A study of singularity formation in vortex-sheet motion by a spectrally accurate vortex method. *J. Fluid Mech.* **244**, 493–526.

SIEGEL, M. 1990 An analytical and numerical study of singularity formation in the Rayleigh–Taylor problem. PhD Thesis, New York University.

SULEM, P., SULEM, C., BARDOS, C. & FRISCH, U. 1981 Finite time analyticity for the two and three dimensional Kelvin–Helmholz instability. *Commun. Math. Phys.* **80**, 485–516.

TANVEER, S. 1993 Singularities in the classical Rayleigh–Taylor flow: Formation and subsequent motion. *Proc. R. Soc. Lond.* A **441**, 501–525.

TRYGGVASON, G., DAHM, W. J. A. & SBEIH, K. Fine-structure of vortex sheet rollup by viscous and inviscid simulation. *Trans. ASME: J. Fluids Engng* **113**, 31–36.